Experimental validation of an efficient strategy for FE model updating and damage identification in tubular structures

Parsa Ghannadi [1], Seyed Sina Kourehli [*2], and Andy Nguyen [3]

[1] *Department of Civil Engineering, Ahar Branch, Islamic Azad University, Ahar, Iran*
https://orcid.org/0000-0001-5441-9243
[2] *Department of Civil Engineering, Azarbaijan Shahid Madani University, Tabriz, Iran*
https://orcid.org/0000-0001-7599-8053
[3] *School of Engineering, University of Southern Queensland, Springfield, QLD 4300, Australia*
https://orcid.org/0000-0001-8739-8207

* Corresponding author: ss.kourehli@azaruniv.ac.ir (S.S Kourehli)

Abstract

Early identification of damages in tubular structures is crucial for their long-term safety and functionality, as they are essential in various modern life applications. Experimental and numerical modal data may slightly differ due to unknown structural characteristics and uncertainties, which are typically addressed using finite element (FE) model updating procedures. Instead of using the Euler-Bernoulli beam element, this paper utilizes the semi-rigidly connected frame element (S-RCFE). By incorporating extra design parameters, such as the end fixity factor of all connections, the S-RCFE offers a unique opportunity to establish a strong agreement between experimental and numerical models through an optimization-based FE model updating procedure. A well-calibrated FE model represents the actual behaviour of the structure and leads to achieving accurate results in the damage detection step. This paper employs the improved grey wolf optimizer (IGWO) and weIghted meaN oF vectOrs (INFO) to minimize 11 objective functions with adjustable coefficients. The statistical investigations reveal that the IGWO effectively minimized five out of six objective functions, which were defined based on the modified total modal assurance criterion (MTMAC). The rest of the objective functions based on the modal assurance criterion (MAC), natural frequency vector assurance criterion (NFVAC), differences in natural frequencies, and a combination of the MAC and NFVAC could not obtain accurate outcomes for the model updating problem. The statistical comparison indicates that the INFO algorithm is unreliable for the FE model updating despite achieving at least one successful result in ten independent runs. The INFO algorithm and the IGWO algorithm demonstrate comparable performance in damage detection. The analysis also shows that the coefficients of MTMAC, alpha and beta, should be adjusted to 0.65 and 1, respectively, to achieve the most accurate damage detection result.

Keywords: FE model updating, Damage detection, Semi-rigidly connected frame element, Improved grey wolf optimizer, Weighted mean of vectors, Modified total modal assurance criterion

1. Introduction

Tubular structures such as offshore jackets, pipes, and circular hollow sections are prone to perforation and corrosion under excessively harsh conditions [1-3]. Serious consequences, including environmental pollution, financial loss, and combustion, might happen if a leak arises in tubular structures [4]. Additionally, considerable marine structures are approaching their service life, and undetected defects potentially result in a sudden structural collapse with destructive repercussions [1, 5]. Non-destructive evaluation of these tubes is crucial to maintain their structural integrity and extend their service life [6]. In addition to traditional visual inspections with the challenge of accessibility for pipelines in deep oceans, local damage detection methods based on X-rays, ultrasonic and acoustic waves, and eddy current have been extensively used [7-9]. Local methods typically need complex instruments, and there are some restrictions, such as the requirement to sense the tested case point by point [8]. Therefore, researchers applied vibration-based [10] structural damage detection techniques as an efficient framework by analyzing the global vibration characteristics such as natural frequencies [11, 12], mode shapes [13-16], mode shape curvatures [17, 18], time-domain responses [19, 20], or frequency response functions [21-23]. Modal properties are sensitive to changes in physical properties, such as stiffness, and structural defects generally appear in stiffness reduction [24]. Therefore, the fundamental concept for vibration-based damage detection approaches is interpreting discrepancies in modal properties [25]. Vibration-based methods might be practical and more beneficial, especially when natural frequencies may be extracted easily using a small number of sensors or perhaps only one [10]. Model-based methods and response-based methods are two categories of vibration-based techniques [25]. Model-based methods employ a numerical model in addition to experimental measurements. In opposition, response-based methods only rely on experimentally measured data [26]. Both damaged elements and their severities are detectable when using model-based methods. Nevertheless, response-based methods are broadly successful in locating the damaged elements [25]. The model-based methods are generally static, and it's not practical to employ them for real-time monitoring because of their disability to track the latest alterations of structural conditions [27]. The capability of the finite element (FE) model to reproduce the dynamic response of real structures is an essential challenge in any model-based damage identification method [28, 29]. Therefore, FE model updating procedures attempt to adjust the numerical model using dynamic or static measurements [30, 31]. According to the literature, the FE model updating methods can be generically divided into two kinds, including iterative methods and non-iterative or direct

methods [32]. Direct methods are the most traditional techniques for updating the stiffness and mass matrices in a single attempt without any iterative strategies, which enables them to be computationally beneficial. The most critical limitation of direct methods is that no direct modifications are made to the physical properties of the FE model, and the numerical model becomes less significant, or its simulation capacity becomes lessened. The updated stiffness and mass matrices might not be positive definite, and symmetric. Therefore, such system matrices are challenging to comprehend physically [30, 32]. In the iterative methods, the uncertain parameters of the structures in the FE model are iteratively adjusted to ensure negligible discrepancies between the calculated and measured dynamic characteristics [33]. Optimization algorithms have been widely employed in recent years to minimize the objective function during an iterative FE model updating method [34-37]. Ghannadi et al. [38-40] comprehensively reviewed the application of three traditional optimizers, including particle swarm optimization (PSO), simulated annealing algorithm, and differential evolution algorithm, in FE model updating and damage detection. They also have analyzed the utilized objective functions and their popularity in recent decades. Various optimizers inspired by natural phenomena and known nature-inspired optimization algorithms have been significantly developed and involved in engineering processes due to their advantages in dealing with highly nonlinear problems and providing satisfactory solutions compared with traditional algorithms [41-43]. Ghannadi and Kourehli implemented several nature-inspired optimization techniques, including the moth-flame algorithm [44], salp swarm algorithm [45], multiverse optimizer [46], and slime mold algorithm [47] for FE model updating and damage identification. The researchers have also reported the successful application of the adaptive hybrid evolutionary firefly algorithm [48], an improved version of the grey wolf optimizer [49], shrimp and goby association search algorithm [50], termite life cycle optimizer [51], and a modified variant of artificial bee colony algorithm [52].

According to the literature, a few studies have focused on FE model updating in tubular structures, most of which are related to offshore wind turbines. El-Borgi et al. [53] conducted a model updating strategy in a laboratory-scaled piping system using a nonlinear iterative algorithm to determine the uncertain parameters of the numerical model until the discrepancies between the measured responses and those calculated from the FE model are minimized. Zhu et al. [54] formulated a two-step damage detection approach for underwater pipeline systems in the statistical framework and validated its efficiency using experimental and numerical examples. The first step quantifies uncertainties of the undamaged numerical model employing

the FE model updating procedure. Then, damaged elements and their severities are identified according to the calibrated model from the first step. A hybrid objective function based on differences in natural frequencies and mode shapes is used in this study. Wang et al. [55] presented an Auto Regressive Moving Average Exogenous model updating approach through the clonal selection algorithm in the time domain, which is applied to damage detection of laboratory-scale pipe laid on the soil. A brief report of attempts to update the experimentally tested pipe has been published by Rajbamshi et al. [56]. The iterative methods in FE model updating and damage detection are generally time-consuming. Therefore, Seguini et al. [57] performed numerical and experimental vibration analyses of intact and cracked pipes. Then, they predicted the crack depth using computationally efficient intelligence techniques, including optimized artificial neural networks by genetic algorithm and PSO [58, 59]. In another study with a similar methodology, Wu et al. [2] identified pipeline damage through an optimized back-propagation neural network using the improved whale optimization algorithm.

As mentioned above, a notable contribution of FE model updating techniques in tubular structures has been practiced with offshore wind turbines. Xu et al. [60] investigated the structural behavior of offshore wind turbines with the monopile foundation by applying an FE model updating technique. In this method, the stiffness of the four horizontal springs, which simulate the interaction between the soil and the offshore wind turbine model, is assigned as the updating parameters. Then, an evolutionary optimization algorithm called estimation of distribution algorithms (EDAs) is employed to minimize two individual objective functions relying on changes in natural frequencies and mode shapes. Ren et al. [61] introduced a framework for FE model updating of monopile-supported offshore wind turbines with an implicit objective function, which considers stiffness and damping of the layered soil as the updating parameters. Abdullahi and Wang [62] implemented a digital twin-like model updating approach using the reduced-order FE model of the laboratory-scale offshore wind turbine, in which EDAs iteratively update the stiffness of the pile-surrounding soil by minimizing two individual objective functions, which contains natural frequencies and mode shapes. Research conducted by Zhang et al. [63] presents a two-step methodology for localizing and quantifying damaged towers or blades in offshore wind turbines. Their proposed strategy attempts to find the damaged components through a global mathematical model. Then, the second step aims to determine the exact location and severity of damaged elements by applying an optimization-based FE model updating method. In this step, the Levenberg-Marquardt algorithm minimizes

an objective function defined through discrepancies in estimated and measured natural frequencies, mode shapes, and mode shape curvatures.

A challenging aspect of model-based methods in structural damage detection is that the FE model of structures holds many degrees of freedom (DOFs). However, for real-world problems, measuring vibration data is practical with only a limited number of DOFs because of the limited number of installed sensors [64]. To address this challenge, the high-dimensional FE model must be reduced by model reduction methods [65, 66], or mode shape expansion techniques must be employed to expand a sparse set of measurements to a larger one [67]. A few studies have been conducted regarding model updating in offshore wind turbines when sparse and incomplete measurements are available. For example, the proposed strategies by Nabiyan et al. [68] and Cong et al. [69] include a mode shape expansion step. Developing mode shape expansion methods is not only related to offshore wind turbines; some efforts have been made to extend it to other onshore and offshore systems, such as the electric submersible pump. The proposed mode shape expansion method by Gutiérrez et al. [70] could successfully function to expand 56 DOFs, which is not measured experimentally in electrical submersible pumps. Implementing the introduced technique to model-based damage detection frameworks is possible in future works.

The present paper proposes a robust FE model updating approach for tubular structures, calibrating an accurate baseline model for subsequent implementation in the damage detection step. This method uses the semi-rigidly connected frame element (S-RCFE) and considers rotational stiffness at each node. The S-RCFE was initially generalized to simulate the semirigid connections of steel-framed structures and applied to system identification [71]. Then, researchers found that S-RCFE enables them to assess joint damage by considering rotational stiffness or, generally speaking, the end fixity factor of each connection as design parameters (DPs) with the assistance of an optimization procedure [72-75]. In the latest study, Ghannadi et al. [76] illustrated that using the FE model updating method through S-RCFE instead of the standard Euler-Bernoulli beam element can yield more precise results in beam-like structures. They found S-RCFE with the end fixity factor of each connection as additional design parameters allow us to calibrate the model perfectly. By considering the research of Ghannadi et al. [76], the following are the main contributions of this paper:

I. This work enriches the FE model updating methods in tubular structures, which is a relatively unexplored topic in the engineering community.

II. This work fills the existing gap between theory and practice by using an experimental pipe model with a length of 2.5 m for validation purposes. Several experimental modal analysis results are statistically studied to determine the variation in modal characteristics and decide how many measured modes should be included in the model updating procedure.

III. The method utilized in this paper is an iterative model updating technique, and the performance of optimization algorithms and objective functions have an essential impact on procedure success. Thus, the capability of two optimization algorithms, including improved grey wolf optimizer (IGWO) and weIghted meaN oF vectOrs (INFO), are statistically investigated. Besides, comprehensive comparative studies examine the efficiency of different objective functions and analyze the sensitivity of objective function's coefficients (alpha and beta) in model updating and damage detection accuracy.

IV. This study compares the convergence curves of the optimization algorithm to explore how incorporating S-RCFE in the model updating process results in superior convergence rates compared to the Euler-Bernoulli beam element.

V. To the author's best knowledge, this paper presents a robust optimization-based model updating approach in tubular structures for the first time.

2. Methodology

This section describes the theoretical basis of structural damage, its definition, and the proposed model-based damage detection approach, including a preliminary model updating step to create an accurate baseline model. The proposed inverse approach employs novel optimization algorithms to minimize the objective functions with adjustable coefficients. This section also includes mathematical formulations of objective functions and local matrices to assemble the FE model using S-RCFE. The mathematical relations of the optimization algorithms are separately presented in Section 3.

2.1. Damage definition

Existing structures may be vulnerable to various conditions, including temperature changes, wind, earthquakes, corrosion, etc. Therefore, these deterioration factors might result in structural damage and lead to sudden collapse, human disaster, and financial loss [49]. Timely identification and repair of possible damages can significantly improve the safety and integrity of structures [77]. In this study, the reduction of elemental stiffness represents structural damage because the deterioration factors mentioned above appear in the reduction of elemental

stiffness. In contrast, the elemental mass remained unchanged before and after the damage [78]. The stiffness matrix for the damaged structure can be calculated as follows:

$$K_d = \sum_{e=1}^{N} (1 - SRF_e) k_e \quad (1)$$

where K_d and k_e are the damaged stiffness matrix and e-th undamaged elemental stiffness matrix, respectively. SRF_e is the stiffness reduction factor of the e-th element, where SRF_e=1 represents the fully damaged state of the e-th element, and SRF_e=0 indicates that the e-th element remains undamaged. The number of elements is shown by N, and SRF is an N-dimensional vector with values between 0 and 1 given as follows [78]:

$$SRF = [SRF_1, SRF_2, \ldots, SRF_N] \quad (2)$$

2.2. Semi-rigidly connected frame element

Perfectly rigid or ideally pinned connections are usually used in traditional structural analysis of frame structures [79]. In contrast to the rigid joints, which restrain rotations, the pinned joints allow theme. In practice, most connections have a moment capacity between perfectly rigid and ideally pinned conditions. Therefore, modern design codes use semi-rigid joints, which define joints based on their actual behavior [71]. The S-RCFE enables us to model joints as partially restrained, improving the model's reality [79]. Only the rotational semi-rigid characteristic is considered for most kinds of connections since the axial and shearing deformations are negligible. The semi-rigid joint is typically modelled using a zero-length rotational spring to consider joint flexibility [73]. As shown in Figure 1, k^j_1 and k^j_2 are the rotational stiffness of the springs at the left and right ends, respectively. k^j_1 and k^j_2 allow rotation to certain degrees according to the end fixity factors J_1 and J_2, respectively.

As mentioned earlier, a few researchers have studied FE model updating approaches in pipes. According to previous studies, the pipe models were generally discretized into several Euler-Bernoulli beam elements [80]. In this study, the FE model of an experimental free-free pipe is assembled using the S-RCFE. Although our studied pipe model lacks bolted connections, we have discretized the pipe into several beam elements with 3-DOFs at each node and considered rotational springs between beam elements. In other words, the S-RCFE enables us to have additional DPs during the optimization-based FE model updating procedure and achieve accurate results because we can consider the end fixity factor of each node as an uncertain parameter in addition to Young's modulus.

Figure 1. Modeling semi-rigidly connected frame element with rotational springs

In Eq. (3) given below, the stiffness matrix of an arbitrary beam with semi-rigid connections is provided [71, 72].

$$[k]=\frac{EI}{L}\begin{bmatrix} \frac{A}{I} & 0 & 0 & -\frac{A}{I} & 0 & 0 \\ & \frac{4(\alpha_1+\alpha_2+\alpha_3)}{L^2} & \frac{2(2\alpha_1+\alpha_2)}{L} & 0 & -\frac{4(\alpha_1+\alpha_2+\alpha_3)}{L^2} & \frac{2(2\alpha_2+\alpha_3)}{L} \\ & & 4\alpha_1 & 0 & -\frac{2(2\alpha_1+\alpha_2)}{L} & 2\alpha_2 \\ & & & \frac{A}{I} & 0 & 0 \\ & & & & \frac{4(\alpha_1+\alpha_2+\alpha_3)}{L^2} & -\frac{2(\alpha_2+2\alpha_3)}{L} \\ sym & & & & & 4\alpha_3 \end{bmatrix} \tag{3}$$

where the following formula determines α_1, α_2, and α_3:

$$\left.\begin{aligned} \alpha_1 &= \frac{3J_1}{4-J_1J_2} \\ \alpha_2 &= \frac{3J_1J_2}{4-J_1J_2} \\ \alpha_3 &= \frac{3J_2}{4-J_1J_2} \end{aligned}\right\} \tag{4}$$

where J_1 and J_2 are the end fixity factors for joints 1 and 2, respectively.

The standard consistent mass matrix [71] of beam elements with rigid ends has been generalized for the existence of semi-rigid connections through the end fixity factors J_1 and J_2 as follows:

$$[m]=\frac{\rho AL}{420D^2}\begin{bmatrix} 140D^2 & 0 & 0 & 70D^2 & 0 & 0 \\ & 4f_1 & 2Lf_2 & 0 & 2f_3 & -Lf_4 \\ & & 4L^2f_5 & 0 & Lf_4 & -L^2f_6 \\ & & & 140D^2 & 0 & 0 \\ & & & & 4f_1 & -2Lf_2 \\ sym & & & & & 4L^2f_5 \end{bmatrix} \tag{5}$$

where the values of $D, f_1, f_2, f_3, f_4, f_5$, and f_6 can be calculated [72] as follows:

$$
\left.\begin{aligned}
&D = 4 - J_1 J_2 \\
&f_1 = 560 + 224J_1 + 32J_1^2 - 196J_2 - 328J_1J_2 - 55J_1^2J_2 + 32J_2^2 + 50J_1J_2^2 + 32J_1^2J_2^2 \\
&f_2 = 224J_1 + 64J_1^2 - 160J_1J_2 - 86J_1^2J_2 + 32J_1J_2^2 + 25J_1^2J_2^2 \\
&f_3 = 560 - 28J_1 - 64J_1^2 - 28J_2 - 184J_1J_2 + 5J_1^2J_2 - 64J_2^2 + 5J_1J_2^2 + 41J_1^2J_2^2 \\
&f_4 = 392J_2 - 100J_1J_2 - 64J_1^2J_2 - 128J_2^2 - 38J_1J_2^2 + 55J_1^2J_2^2 \\
&f_5 = 32J_1^2 - 31J_1^2J_2 + 8J_1^2J_2^2 \\
&f_6 = 124J_1J_2 - 64J_1^2J_2 - 64J_1J_2^2 + 31J_1^2J_2^2
\end{aligned}\right\} \tag{6}
$$

2.3. Optimization-based FE model updating and damage detection procedure

The material and connections between structural elements are subject to many idealizations, discretizations, assumptions, and epistemic uncertainties, and numerical models often exhibit significant uncertainty. FE model updating methods attempt to minimize the gap between experimental and theoretical calculations by adjusting the uncertain parameters [81]. FE model updating procedures are often formulated as an optimization framework by minimizing an objective function. The differences between numerically calculated dynamic characteristics (natural frequencies and mode shapes) and those measured values from the experiment define the objective function [82]. Previous research has presented a wide variety of objective functions [83]. However, properly selecting an appropriate objective function may significantly influence the effectiveness of any model updating procedure [84]. This study conducts a detailed comparison to address the significant impact of objective functions on model updating of the free-free pipe and find the most sensitive objective functions. In addition to comparing the single and hybrid objective functions, this paper investigates the sensitivity of objective functions' coefficients (alpha and beta).

The modified total modal assurance criterion (MTMAC) is a robust objective function that combines the modal assurance criterion (MAC) with natural frequencies to meet the updating requirements for both mode shapes and natural frequencies [85]. In the model updating process in this study, the end fixity factor for all joints and Young's modulus for all elements are considered unknown parameters (X). Considering n modes, the objective function based on MTMAC [86] is formulated as follows:

$$
f_{MTMAC}(X) = \alpha\left(\sum_{i=1}^{n}\left(1 - MTMAC_i(X)\right)^{\beta}\right) \tag{7}
$$

where $MTMAC_i(X)$ can be defined as follows:

$$
MTMAC_i(X) = \frac{MAC_i\left(\{\phi_i^m\},\{\phi_i^c(X)\}\right)}{1 + \left|\dfrac{\left(\omega_i^m\right)^2 - \left(\omega_i^c(X)\right)^2}{\left(\omega_i^m\right)^2 + \left(\omega_i^c(X)\right)^2}\right|} \tag{8}
$$

where ω_i^m and $\omega_i^c(X)$ are the i-th measured and calculated natural frequencies, respectively. The MAC function returns a value of one if the compared mode shapes are correlated and zero if they are uncorrelated [87]. MAC values between the i-th calculated and measured mode shapes, $\phi_i^c(X)$ and ϕ_i^m, are obtained as follows:

$$MAC_i(X) = \frac{\left|\{\phi_i^m\}^T \{\phi_i^c(X)\}\right|^2}{\left(\{\phi_i^c(X)\}^T \{\phi_i^c(X)\}\right)\left(\{\phi_i^m\}^T \{\phi_i^m\}\right)} \tag{9}$$

The utilized dynamic characteristics (natural frequencies and mode shapes) in Eqs. (8 and 9) can be calculated [88] by solving the following eigenvalue equation:

$$K\phi_i = \omega_i^2 M \phi_i, \qquad i=1, 2, \ldots, n \tag{10}$$

where M and K are the mass and stiffness matrices, respectively. Additionally, n displays the number of DOFs.

The presented objective functions in Eqs. (11 and 12) are only relying on natural frequencies [47, 76].

$$f_{frequency}(X) = \alpha\left(\sum_{i=1}^{n}\left(\left(\omega_i^m - \omega_i^c(X)\right)^2 / \left(\omega_i^m\right)^2\right)^{\beta}\right) \tag{11}$$

$$f_{NFVAC}(X) = \alpha\left(\sum_{i=1}^{n}\left(1 - NFVAC_i(X)\right)^{\beta}\right) \tag{12}$$

where $NFVAC(X)$ can be computed [89] as follows:

$$NFVAC(X) = \frac{\left|\{F^m\}^T \{F^c(X)\}\right|^2}{\left(\{F^c(X)\}^T \{F^c(X)\}\right)\left(\{F^m\}^T \{F^m\}\right)} \tag{13}$$

where $F^c(X)$ the calculated natural frequency vector and F^m is the measured natural frequency vector. The natural frequency vector assurance criterion (NFVAC) states that when the calculated values are close to one, it indicates a strong correlation between two arbitrary natural frequency vectors. The following equation can also be used to establish the natural frequency vector:

$$F = \begin{Bmatrix} \omega_1 \\ \vdots \\ \omega_n \end{Bmatrix}_{n\times 1} \tag{14}$$

Mode shapes are widely used characteristics to formulate objective functions, and the MAC function is typically utilized to evaluate the correlation between the measured and calculated mode shapes. The objective function based on MAC [90] is expressed as follows:

$$f_{MAC}(X)=\alpha\left(\sum_{i=1}^{n}\left(1-MAC_i(X)\right)^{\beta}\right) \tag{15}$$

Eq.(16) gives a hybrid objective function combining natural frequency and mode shape terms. Certain engineering problems may be solved efficiently through multi-objective optimization and minimizing multiple objectives simultaneously. The weighted sum technique integrates all the multi-objective functions into a single scalar and creates a weighted composite objective function [91]. In Eq. (16), the coefficients α and β may be essential in achieving optimal model updating results. However, It can be challenging to determine the appropriate coefficients before running the optimization algorithm and analyzing initial results. A typical approach to address this difficulty is to weigh all terms equally, while this approach may cause sub-optimal identification results [90]. Therefore, trials and errors are needed to find optimal values of α and β.

$$f_{MAC-NFVAC}(X)=\alpha\left(\sum_{i=1}^{n}\left(1-MAC_i(X)\right)\right)+\beta\left(\sum_{i=1}^{n}\left(1-NFVAC_i(X)\right)\right) \tag{16}$$

The optimization algorithms minimize the above-mentioned objective functions while exploring the optimal properties of the dynamic system. As a result, the obtained optimal solution perfectly reflects the modal characteristics and can be contributed to establishing the baseline model, which represents a structure's actual behaviors. The baseline model can be compared with the target structure in different damaged scenarios by minimizing objective functions and identifying the damage locations and their severities [92]. In this regard, two objective functions based on MTMAC and natural frequencies are defined as follows:

$$f_{MTMAC}(SRF)=\alpha\left(\sum_{i=1}^{n}\left(1-MTMAC_i(SRF)\right)^{\beta}\right), \qquad 0\le SRF\le 1 \tag{17}$$

$$f_{frequency}(SRF)=\alpha\left(\sum_{i=1}^{n}\left(\left(\omega_i^m-\omega_i^c(SRF)\right)^2/\left(\omega_i^m\right)^2\right)^{\beta}\right), \qquad 0\le SRF\le 1 \tag{18}$$

Natural frequencies are comparatively easy to measure, and frequency-based objective functions benefit from being practical in real-world applications. However, frequency change methods have at least two drawbacks in detecting structural damage. First, severe damage might result in minimal changes to natural frequencies, especially for large-scale structures, and these modifications may be undetectable due to measurement errors. Second, temperature variations might cause uncertainty in the measured frequencies [93]. Unlike natural frequency changes, variations in mode shapes are considerably sensitive to local damage. However, involving mode shapes has certain disadvantages as well. First, damages are local phenomena

and may not substantially affect the lower mode shapes, which are often measured by field vibration tests. Second, environmental noise, erroneous sensor placements, or ambient loads may affect the extracted mode shapes. Third, the accuracy of the damage detection process may be significantly impacted by the number and arrangement of installed sensors [94]. Figure 2 illustrates the flowchart of the damage detection strategy.

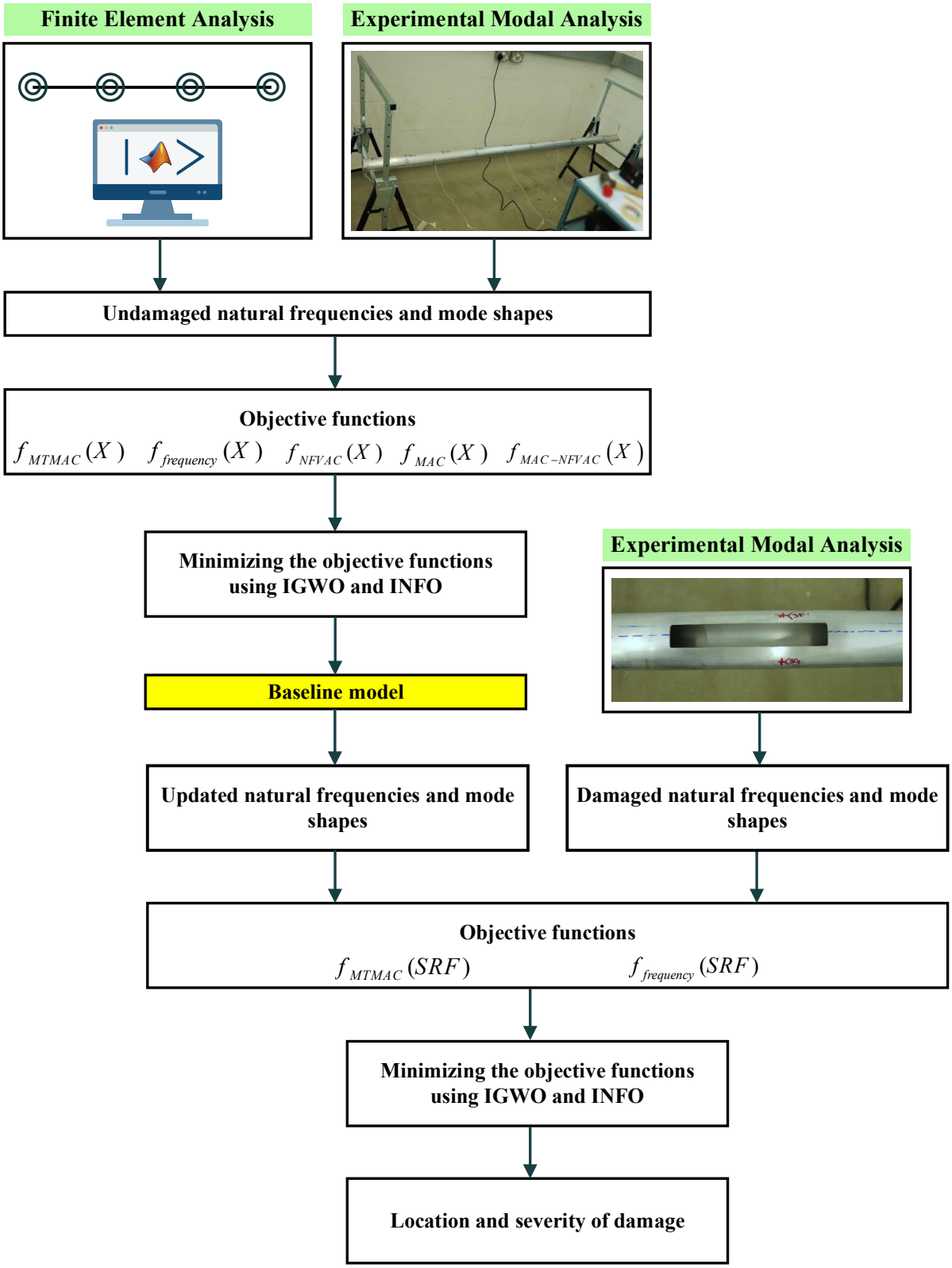

Figure 2. Flowchart of the damage detection strategy (experimental model courtesy of Obukho E. Esu)

3. Optimization algorithms

Two optimization algorithms, including improved grey wolf optimizer (IGWO) and weIghted

meaN oF vectOrs (INFO), are employed to minimize the objective functions during FE model updating and damage detection procedures. This section briefly describes utilized optimizers and their mathematical relations to minimize objective functions.

3.1. weIghted meaN oF vectOrs (INFO)

Ahmadianfar *et al*. [95] introduced the INFO technique as an efficient optimization algorithm in 2022. INFO is a modified weight mean approach that uses three key operations to update the positions of the vectors, which can contribute to creating a potent framework. Through a series of iterative generations, the INFO algorithm finds the optimal solution. In each generation, the following three operators update the positions of the vectors:

- Step1: Updating rule
- Step2: Vector combining
- Step3: Local search

INFO is a population-based optimization technique that determines the weighted mean for a group of vectors in the search space. The INFO algorithm involves a population of n vectors within a search space of D dimensions [95]. According to Eq. (19), this algorithm uses a random generation method [96] to produce the initial population:

$$X_n = X_{\min} + rand\,(0,1).\left(X_{\max} - X_{\min}\right) \tag{19}$$

where X_n represents the n-th vector, *rand* (0, 1) denotes a random number in the range [0, 1], and each problem's solution domain has upper and lower bounds, X_{max} and X_{min}.

The updating rule operator in the INFO algorithm expands the population's broadness throughout the search procedure. This operator employs the weighted mean of the vectors to generate new vectors. The following scheme [96] defines the updating rule in the INFO algorithm:

if $rand < 0.5$

$$z1_l^{iter} = x_l^{iter} + \sigma \times MeanRule + randn \times \frac{\left(x_{bs} - x_{a1}^{iter}\right)}{\left(f\left(x_{bs}\right) - f\left(x_{a1}^{iter}\right) + 1\right)}$$

$$z2_l^{iter} = x_{bs} + \sigma \times MeanRule + randn \times \frac{\left(x_{a1}^{iter} - x_b^{iter}\right)}{\left(f\left(x_{a1}^{iter}\right) - f\left(x_{a2}^{iter}\right) + 1\right)} \tag{20}$$

else

$$z1_l^{iter} = x_a^{iter} + \sigma \times MeanRule + randn \times \frac{\left(x_{a2}^{iter} - x_{a3}^{iter}\right)}{\left(f\left(x_{a2}^{iter}\right) - f\left(x_{a3}^{iter}\right) + 1\right)}$$

$$z2_i^{iter} = x_{bt} + \sigma \times MeanRule + randn \times \frac{\left(x_{a1}^{iter} - x_{a2}^{iter}\right)}{\left(f\left(x_{a1}^{iter}\right) - f\left(x_{a2}^{iter}\right) + 1\right)}$$

end

where the new vectors in the *g*-th generation are shown by $z1_l^{iter}$ and $z2_l^{iter}$; σ defines the scaling rate of a vector according to Eq. (21):

$$\sigma = 2\alpha \times rand - \alpha \tag{21}$$

where alpha is determined relying on the exponential function defined by Ahmadianfar *et al*. [95].

In the INFO algorithm, two computed vectors by updating rule ($z1_l^{iter}$ and $z2_l^{iter}$) are integrated with vector x_l^{iter} to increase the population's diversity. In other words, the main concept behind the vector combining step is to upgrade the local search capability and generate a new effective vector [95, 96]:

$$\begin{aligned}
&\textbf{\textit{if}}\ rand < 0.5\\
&\quad \textbf{\textit{if}}\ rand < 0.5\\
&u_l^{iter} = z1_l^{iter} + \mu.\left|z1_l^{iter} - z2_l^{iter}\right|\\
&\quad \textbf{\textit{else}}\\
&u_l^{iter} = z2_l^{iter} + \mu.\left|z1_l^{iter} - z2_l^{iter}\right|\\
&\quad \textbf{\textit{end}}\\
&\textbf{\textit{else}}\\
&u_l^{iter} = x_l^{iter}\\
&\textbf{\textit{end}}
\end{aligned} \tag{22}$$

where u_l^{iter} is the *g*-th generated vector using the vector combining, and μ equals 0.05×rand*n*.

The local search step attempts to prevent the INFO algorithm from entrapping into locally optimal solutions [95]. The local operator considers the global position (x_{best}^{g}) and the mean-based rule to enhance the search and exploitation abilities along with convergence to global optima [95, 96]. Therefore, a new vector is generated around (x_{best}^{g}) using this operator, as given in Eq. (23):

$$\begin{aligned}
&\textbf{\textit{if}}\ rand < 0.5\\
&\quad \textbf{\textit{if}}\ rand < 0.5\\
&u_l^{iter} = x_{bs} + randn \times \left(MeanRule + randn \times \left(x_{bs}^{iter} - x_{a1}^{iter}\right)\right)\\
&\quad \textbf{\textit{else}}\\
&u_l^{iter} = x_{rnd} + randn \times \left(MeanRule + randn \times \left(\upsilon_1 \times x_{bs} - \upsilon_2 \times x_{rnd}\right)\right)\\
&\quad \textbf{\textit{end}}\\
&\textbf{\textit{end}}\\
&x_{rnd} = \phi \times x_{avg} + (1-\phi) \times \left(\phi \times x_{bt} + (1-\phi) \times x_{bs}\right)\\
&x_{avg} = \frac{\left(x_a + x_b + x_c\right)}{3}
\end{aligned} \tag{23}$$

where ϕ generates a random number between 0 and 1; and x_{rnd} produces a new solution by

randomly combining the components of the solutions based on x_{avg}, x_{bt}, and x_{bs}. This makes the INFO algorithm's randomization aspect more pronounced for improved solution space searching [95]. In Eq.(23), v1 and v2 are two random numbers, which generates as follows:

$$\upsilon_1 = \begin{cases} 2 \times rand & if\ \rho > 0.5 \\ 1 & otherwise \end{cases} \tag{24}$$

$$\upsilon_2 = \begin{cases} rand & if\ \rho < 0.5 \\ 1 & otherwise \end{cases} \tag{25}$$

where ρ represents a random number between 0 and 1.

3.2. Improved grey wolf optimizer (IGWO)

The grey wolf optimizer (GWO) algorithm is inspired by grey wolves' hunting strategies and social leadership, which are observed in their natural habitat. The GWO employs α, β, and δ to lead ω wolves to thoroughly explore spaces with promising possibilities and discover the most optimal solution [97]. However, this process may lead to a potential drawback and cause a possibility of becoming trapped in local optima. Additionally, the algorithm's tendency to reduce population variety may converge to local optima rather than exploring a more comprehensive range of solutions. Nadimi-Shahraki et al. [98] proposed the improved grey wolf optimizer (IGWO) to tackle these limitations according to the following three phases:

Initialization phase: The distribution of N wolves in the search space between [l_i, u_j] is determined randomly [98] using the following equation:

$$X_{ij} = l_j + rand_j\,[0,1] \times \left(u_j - l_j\right), i \in [1, N], j \in [1, D] \tag{26}$$

A vector of real values $X_i\,(t) = \{x_{i1}, x_{i2}, \ldots, x_{iD}\}$ represents the position of the i-th wolf in the t-th iteration, where D corresponds to the problem's dimensionality.

Movement phase: Grey wolves are not only known for their group hunting skills but also for their remarkable ability to engage in individual hunting. This unique behaviour contributes to enhancing and refining the basic GWO. The IGWO has an advanced movement strategy incorporating the dimension learning-based hunting (DLH) search method alongside the canonical GWO search strategy. When using the DLH search method, every wolf is learned by its neighbouring wolves as a potential candidate for a new position. The following equation [98] calculates the dimension of the wolf's new position:

$$X_{i-DLH,d}\,(t+1) = X_{i,d}\,(t) + rand \times \left(X_{n,d}\,(t) - X_{r,d}\,(t)\right) \tag{27}$$

where the d-th dimension of $X_{i\text{-}DLH,\,d}\,(t+1)$ is determined based on the d-th dimension of a

randomly selected neighboring variable $X_{n,d}(t)$ and a randomly selected wolf $X_{r,d}(t)$ from a population. Additional information has been presented by Nadimi-Shahraki et al. [98].

Selecting and updating phase: In this phase, the superior candidate is initially identified by comparison of the fitness values of candidates $X_{i-GWO}(t+1)$ and $X_{i-DLH}(t+1)$, as calculated using Eq. (28). If the selected candidate's fitness value is less than $X_i(t)$, $X_i(t)$ is updated by the selected candidate to determine the new position of $X_i(t+1)$. However, if the fitness value is greater or equal to $X_i(t)$, $X_i(t)$ remains unchanged [98].

$$X(t+1)=\begin{cases} X_{i-GWO}(t+1), & if\ f\left(X_{i-GWO}\right)<f\left(X_{i-DLH}\right) \\ X_{i-DLH}(t+1) & otherwise \end{cases} \tag{28}$$

Where $X_{i-GWO}(t+1)$ is the first candidate [98] for the new position of wolf $X_i(t)$ and can be determined from the canonical GWO search strategy presented by Mirjalili et al. [97].

4. Experimental example

The experimental example is a free-free aluminium pipe with geometrical and material properties listed in Table 1. The modal analysis has been performed on intact and damaged conditions at the Structural Engineering Laboratory of the University of Surrey, Guildford, UK [99]. A photograph and schematic of the experiment procedure are illustrated in Figures 3 and 4, respectively. The experimental pipe model has been suspended by two tension springs at 40 mm from the left and right ends to simulate free-free boundary conditions, as schematically illustrated in Figure 4. Six uniaxial accelerometers have been attached to the pipe at locations 2.5, 430, 980, 1525, 2080, and 2497.5 mm from the left end to measure accelerations and perform modal analysis (see Figure 4). The opposite end of each accelerometer has also been wired to a channel of data acquisition chassis. One channel in the chassis has been exclusively considered for connecting the modal hammer. In the modal tests, test specimens must be excited to induce vibration. The modal hammer is a widely used method to implement this excitation. Details of the modal testing setup and data acquisition system are presented in Figure 5. The sensitivity of modal properties to different hammer impacts has been analyzed to investigate the repeatability of the extracted characteristics from modal analysis. According to Figure 4, six hammer impact locations on the experimental pipe have been considered, and data measurements have been conducted three times per impact location. The direction of the hammer impacts (90˚ –270˚) is shown in Figure 4. A dataset of 18 independent measurements collected for the undamaged pipe is listed in Table 2. It can be observed from Figure 6 that the standard deviations for the first four natural frequencies are extremely close to zero.

Consequently, the extracted natural frequencies from the modal test are repeatable for 18 independent measurements of undamaged cases.

A section of pipe has been removed through cutting to cause a damaged scenario artificially, as shown in Figure 3. Achieving cuts with precisely right angles is not feasible, necessitating a tolerance of a 2 mm radius during the cutting process to account for the rounding of sharp edges. Figure 4 shows a 200 mm removed section between 837.5 mm and 1037.5 mm from the left end. Similar to the undamaged condition, the sensitivity of modal properties to hammer impact locations and sensor arrangements has been analyzed. Table 2 lists four independent measurements for the damaged scenario. According to Figure 6, it is clear that the natural frequencies are repeatable for the first five modes with minor standard deviations.

The FE model consists of 13 frame elements that are semi-rigidly connected, and each of these elements is restricted by two rotational springs (k^j_1, k^j_2). The coordinates of rotational springs ($\mathbf{Ck}^j_1$, $\mathbf{Ck}^j_2$) for each element are presented in Table 3. Table 3 also presents the location of damage, which exists between 837.5 mm and 1037.5 mm from the left end and includes the fifth and sixth elements.

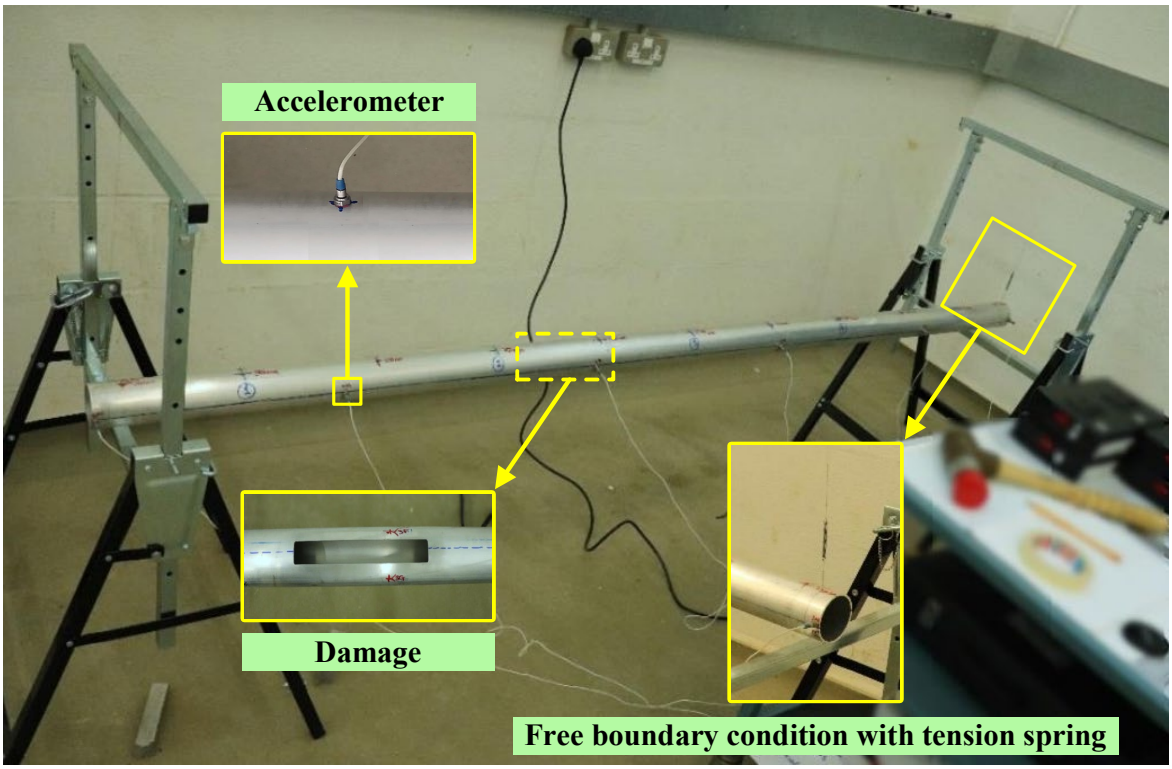

Figure 3. A photograph of modal testing on the experimental pipe with free-free boundary conditions [99]

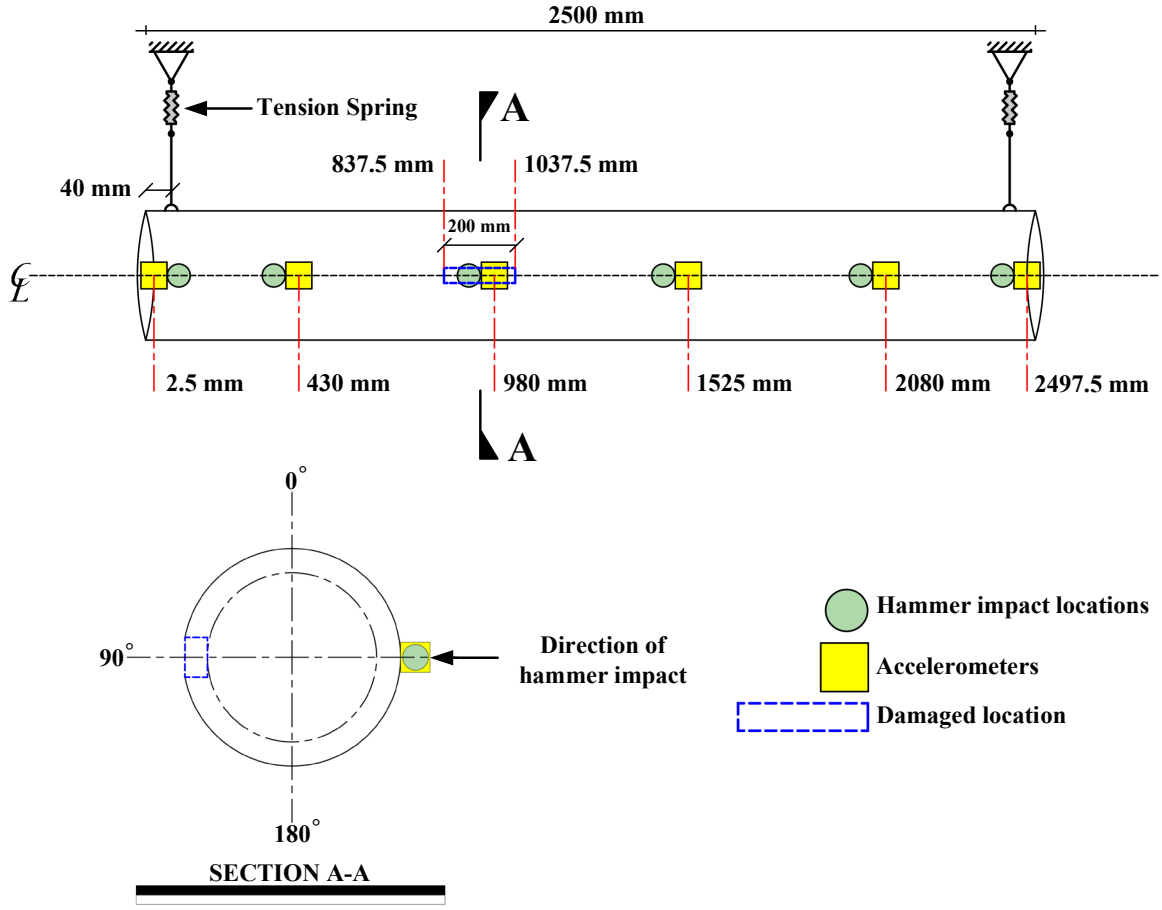

Figure 4. A schematic of modal testing on the experimental pipe with free-free boundary conditions

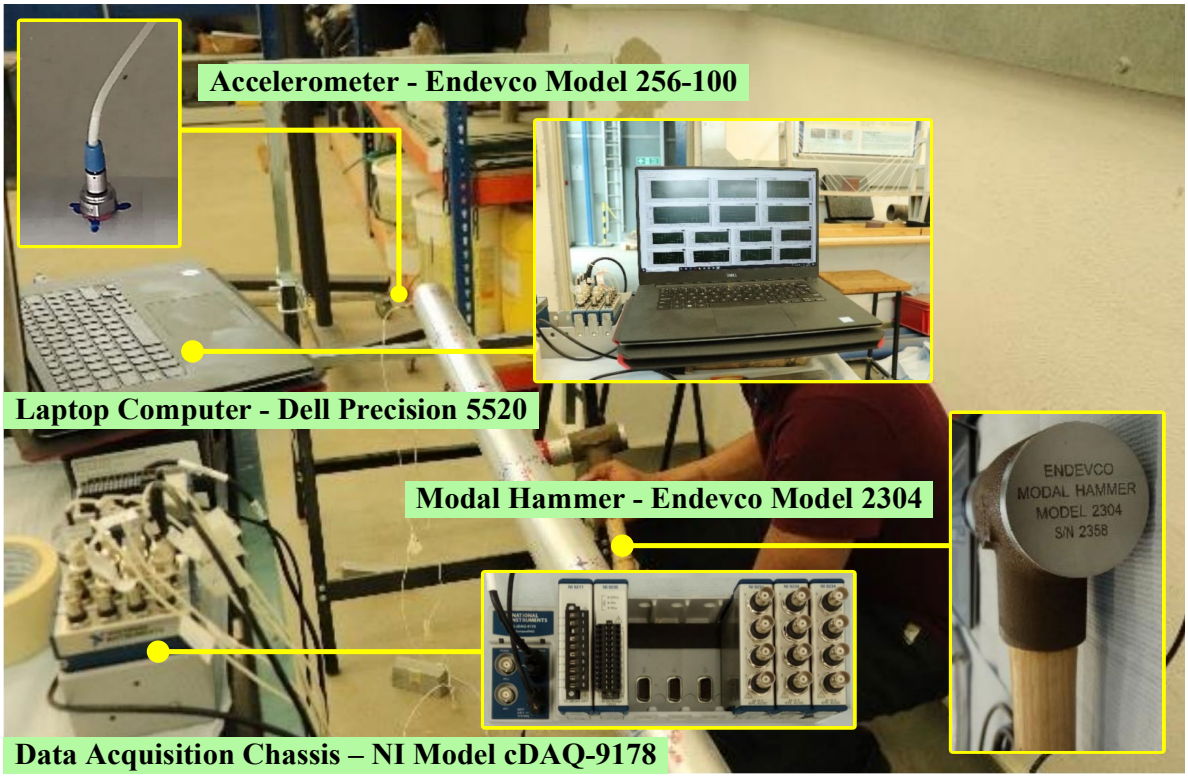

Figure 5. Details of modal testing setup on the experimental pipe with free-free boundary conditions [99]

Table 1. Geometrical and material properties of experimental pipe

Properties	Value
Elasticity modulus (MPa)	72000
Outside diameter (mm)	76.2
Wall thickness (mm)	3.25
Poisson's ratio	0.3
Density (kg/m^3)	2700
Length (mm)	2500
Cross-sectional area (m^2)	7.448×10^{-4}
Second moment of area (m^4)	4.965×10^{-7}

Table 2. The extracted natural frequencies (Hz) from different measurement cases

Measurement Case	Mode					
	1	2	3	4	5	6
Undamaged #1	75	204	394	636	1053	1260
Undamaged #2	75	204	394	636	928	1257
Undamaged #3	75	204	394	636	1031	1267
Undamaged #4	75	204	394	636	927	1256
Undamaged #5	75	204	394	636	928	1257
Undamaged #6	75	204	394	636	928	1255
Undamaged #7	75	204	394	636	928	1256
Undamaged #8	75	204	394	636	927	1257
Undamaged #9	75	204	394	636	927	1257
Undamaged #10	75	204	394	636	928	1258
Undamaged #11	75	204	394	636	927	1260
Undamaged #12	75	204	394	636	928	1254
Undamaged #13	75	204	394	636	928	1250
Undamaged #14	75	204	394	636	928	1257
Undamaged #15	75	204	394	636	927	1260
Undamaged #16	75	204	394	636	928	1259
Undamaged #17	75	204	394	636	928	1258
Undamaged #18	75	204	394	636	928	1258
Damaged #1	72	201	392	625	917	1255
Damaged #2	72	201	392	624	917	1262
Damaged #3	72	201	392	625	917	1257
Damaged #4	72	201	392	625	917	1256

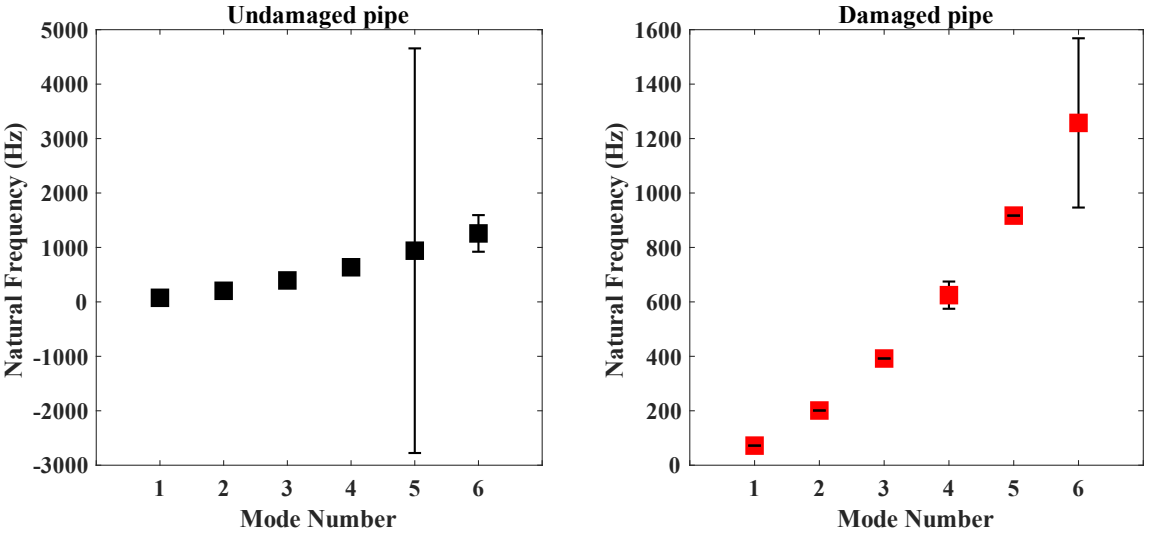

Figure 6. The mean values and standard deviations of extracted natural frequencies from different measurements (error bars were scaled up by a factor of 100 and displayed exaggeratedly on the plot)

Table 3. The coordinates of rotational springs for each element and the damaged location on the experimental pipe

Length of pipe (m)	2.5												
Element number	1	2	3	4	5	6	7	8	9	10	11	12	13
Coordinates of rotational springs **[Ck^j_1, Ck^j_2]**	[0, 0.2]	[0.2, 0.43]	[0.43, 0.63]	[0.63, 0.77]	[0.77, 0.98]	[0.98, 1.18]	[1.18, 1.38]	[1.38, 1.525]	[1.525, 1.7250]	[1.7250, 1.9250]	[1.9250, 2.08]	[2.08, 2.28]	[2.28, 2.5]
Damaged location (m)					0.8375 to 1.0375								

5. Results and discussion

This section presents the statistical results (mean values and standard deviations of 10 independent runs) to investigate the performance of optimization algorithms (IGWO and INFO) in FE model updating and structural damage identification. The maximum number of iterations and search agents are important parameters during optimization and may affect the solutions. Therefore, this paper considers two sets of values for the maximum number of iterations and search agents. Table 4 presents the optimization algorithms' settings; LB and UB represent the lower and upper bounds, restricting search space. For example, optimization algorithms attempt to find solution vector X includes ±30% of initial DPs (Young's modulus and the end fixity factor of semi-rigidly connected beam elements). Regarding the damage detection step, *SRF* is a vector with components ranging between 0 and 1, representing each element's damage severity.

This paper uses statistical comparisons to find the efficient objective function and optimal coefficients (alpha and beta) for adjusting the objective function's best performance. Tables 5 to 10 comprehensively compare the statistical results regarding employed optimization algorithms, objective functions, and their coefficients for FE model updating. The sensitivity of objective functions' coefficients and optimization algorithms' settings for damage detection are also in Figures 8 to 11. The following are comprehensive discussions on the provided results in Tables 6 to 11 and Figures 8 to 11.

Table 4. The IGWO and INFO algorithms' settings

FE model updating	Search agent = 70	$LB \leq DPs \times (1-X) \leq UB$ LB = - 0.3 UB = 0.3
	Maximum iteration = 500	
	Search agent = 10^2	
	Maximum iteration = 10^3	
Damage detection	Search agent = 70	$LB \leq SRF \leq UB$ LB = 0 UB = 1
	Maximum iteration = 500	
	Search agent = 10^2	
	Maximum iteration = 10^3	

Table 5 provides the statistical comparison of FE model updating when employing IGWO as an optimization algorithm (search agent=70 and maximum iteration=500) and defining different objective functions with adjustable coefficients ($f_{MTMAC}(X)$, $f_{frequency}(X)$, $f_{MAC}(X)$, $f_{NFVAC}(X)$, $f_{MAC\text{-}NFVAC}(X)$). It's worth emphasizing that the poor results are indicated in bold. In the FE model updating problems, it is essential to calibrate the numerical model to obtain minor differences between calculated and experimental natural frequencies. At the same time, the calculated MAC values between experimental and numerical mode shapes must also indicate a strong correlation. When defining objective functions based on MTMAC, updated FE models could produce natural frequencies with negligible differences compared to experimental natural frequencies. Additionally, strong correlations have been reported between experimental and updated mode shapes, as shown in Table 5. The results revealed that the accuracy of model updating is not sensitive to objective functions' coefficients. However, a relatively minor error can be seen in the fourth mode when adopting 5 and 1 for alpha and beta, respectively.

When forming objective functions based on changes in natural frequencies ($f_{frequency}(X)$), updated models could only provide accurate natural frequencies, and mode shape correlation is unsatisfactory. The mode shape correlation could not be increased even with the alpha and beta changes.

The results of FE model updating by minimizing an objective function based on MAC indicate the complete agreement between updated and experimental mode shapes due to the MAC values equal to 1.0000 for the first four modes. Notably, considerable differences (minimum=1.6643E+01% and maximum=1.8575E+01%) exist between the experimental natural frequencies and the updated ones.

The FE model updating results demonstrate that defining objective function based on NFVAC could not provide a strong agreement between experimental and updated models. There are relatively large errors with major standard deviations in updated natural frequencies. Besides, calculated MAC values between experimental and updated mode shapes are unfavourable (minimum MAC=0.9613 at the first mode and maximum MAC= 0.9970 at the fourth mode).

The latest section of Table 5 shows that combining two objective functions, $f_{MAC}(X)$ and $f_{NFVAC}(X)$, could not reduce differences between experimental and updated natural frequencies, and there are still significant errors (minimum= 1.5155E+01% and maximum= 1.6362E+01%) for all four modes. Although a strong correlation is observed between updated and experimental mode shapes (minimum MAC= 0.9999 and maximum MAC=1.0000), that is only sufficient if the accuracy of natural frequencies improves.

Table 5. Statistical results of FE model updating - IGWO (search agent=70 and maximum iteration=500)

Mode		1	2	3	4
Experimental f (Hz)		75	204	394	636
$f_{MTMAC}(X)$ $\alpha=1,\beta=1$	mean f (Hz)	74.9995	203.9999	393.9974	636.0064
	std f	1.3525E-03	5.1386E-03	4.6923E-03	1.7753E-02
	error f (%)	6.4422E-04	2.6883E-05	6.4925E-04	1.0026E-03
	mean MAC	0.9997	0.9996	0.9998	0.9999
	std MAC	1.2521E-04	8.3717E-05	7.2010E-05	8.6910E-05
$f_{MTMAC}(X)$ $\alpha=1,\beta=0.5$	mean f (Hz)	75.0004	203.9957	394.0003	636.0015
	std f	1.2736E-03	4.4655E-03	7.0495E-03	9.2709E-03
	error f (%)	5.2562E-04	2.0855E-03	6.7608E-05	2.3433E-04
	mean MAC	0.9997	0.9997	0.9998	0.9999
	std MAC	1.1832E-04	1.5164E-04	1.5493E-04	7.2018E-05
$f_{MTMAC}(X)$ $\alpha=1,\beta=2$	mean f (Hz)	75.0001	203.9993	394.0020	635.9957
	std f	1.1052E-03	1.3065E-03	8.6056E-03	3.3711E-02
	error f (%)	1.5860E-04	3.4274E-04	5.0025E-04	6.7682E-04
	mean MAC	0.9997	0.9996	0.9997	0.9998
	std MAC	8.3262E-05	7.9826E-05	8.4485E-05	1.0992E-04
$f_{MTMAC}(X)$ $\alpha=0.5,\beta=1$	mean f (Hz)	75.0005	204.0014	394.0050	635.9994
	std f	3.3515E-03	5.6345E-03	4.5859E-03	2.9850E-03
	error f (%)	6.2354E-04	6.7929E-04	1.2570E-03	1.0196E-04
	mean MAC	0.9994	0.9995	0.9998	1.0000
	std MAC	1.4381E-04	2.6992E-04	1.1536E-04	3.5016E-05
$f_{MTMAC}(X)$ $\alpha=2,\beta=1$	mean f (Hz)	75.0000	204.0010	394.0016	636.0136
	std f	5.9638E-04	2.0824E-03	2.2954E-02	4.9888E-02
	error f (%)	6.3371E-05	4.7076E-04	3.9391E-04	2.1310E-03
	mean MAC	0.9997	0.9997	0.9997	0.9996
	std MAC	5.3663E-05	9.9673E-05	1.7273E-04	2.9359E-04
$f_{MTMAC}(X)$ $\alpha=5,\beta=1$	mean f (Hz)	74.9999	203.9986	394.0316	637.3264
	std f	3.5734E-04	6.0896E-03	1.5545E-01	**1.0299E+01**
	error f (%)	7.1009E-05	7.0925E-04	8.0199E-03	**2.0855E-01**
	mean MAC	0.9998	0.9996	0.9994	**0.9980**
	std MAC	6.9150E-05	1.7195E-04	4.1178E-04	2.2993E-03
$f_{frequency}(X)$ $\alpha=1,\beta=2$	mean f (Hz)	74.9994	204.0023	393.9977	636.0069
	std f	2.0087E-03	5.8506E-03	1.3460E-02	1.1147E-02
	error f (%)	8.2656E-04	1.1517E-03	5.7972E-04	1.0863E-03
	mean MAC	**0.9538**	**0.9926**	**0.9731**	**0.9920**
	std MAC	6.0305E-02	6.8696E-03	2.5482E-02	6.8604E-03
$f_{frequency}(X)$ $\alpha=2,\beta=2$	mean f (Hz)	75.0002	204.0001	394.0015	636.0118
	std f	1.0353E-03	3.1083E-03	6.3711E-03	2.7960E-02
	error f (%)	2.2355E-04	5.1976E-05	3.9163E-04	1.8500E-03
	mean MAC	**0.9395**	**0.9942**	**0.9867**	**0.9980**
	std MAC	1.1144E-01	9.5603E-03	1.4877E-02	1.3986E-03
$f_{MAC}(X)$ $\alpha=1,\beta=2$	mean f (Hz)	61.9876	166.1064	328.4266	521.1297
	std f	**1.2026E+01**	**3.1600E+01**	**6.4983E+01**	**1.0923E+02**
	error f (%)	**1.7350E+01**	**1.8575E+01**	**1.6643E+01**	**1.8061E+01**
	mean MAC	1.0000	1.0000	1.0000	1.0000
	std MAC	1.0027E-05	2.9676E-06	4.3434E-06	6.9137E-06
$f_{NFVAC}(X)$ $\alpha=1,\beta=1$	mean f (Hz)	75.7581	206.0694	397.9975	642.4422
	std f	**6.2996E+00**	**1.7138E+01**	**3.3101E+01**	**5.3417E+01**
	error f (%)	**1.0108E+00**	**1.0144E+00**	**1.0146E+00**	**1.0129E+00**
	mean MAC	**0.9613**	**0.9949**	**0.9853**	**0.9970**
	std MAC	4.2671E-02	3.0739E-03	1.1965E-02	3.8361E-03
$f_{MAC\text{-}NFVAC}(X)$ $\alpha=1,\beta=1$	mean f (Hz)	63.2046	170.6213	334.2887	537.1051
	std f	**3.6061E+00**	**9.8855E+00**	**1.9103E+01**	**3.1152E+01**
	error f (%)	**1.5727E+01**	**1.6362E+01**	**1.5155E+01**	**1.5550E+01**
	mean MAC	0.9999	0.9999	1.0000	1.0000
	std MAC	1.3222E-05	4.4228E-06	4.7509E-06	1.5362E-06

Table 6 presents a statistical investigation of the effectiveness of FE model updating using IGWO (search agent=10^2 and maximum iteration=10^3) as an optimization algorithm. This table includes the outcomes of various objective functions featuring adjustable coefficients similar to those arrangements presented in Table 5.

According to Table 5, we recently found that the results of FE model updating based on minimizing MTMAC are highly accurate, and outcomes are almost insensitive to varying coefficients. However, there is only an opportunity to improve the MAC values (0.9980) and decrease the standard deviation (1.0299E+01) for the fourth mode when using MTMAC (alpha=5 and beta=1) as the objective function. As Table 6 shows, increasing the search agent to 10^2 and the maximum number of iterations to 10^3 could improve the MAC value (0.9990) and decrease the standard deviation to 1.5245E+00. However, the error on natural frequencies (1.7580E-01) is still remarkable.

We previously found from Table 5 that the minimizing objective function relying on $f_{frequency}(X)$ could only provide good agreements regarding natural frequencies. The paper examines whether changing algorithms' settings can enhance the Mac values. However, based on the analysis presented in Table 6, it can be concluded that there was no significant improvement in MAC values despite increasing the maximum number of iterations and the search agent. Additionally, after adjusting alpha and beta to 2, there were substantial inaccuracies in the natural frequencies. The extremely large standard deviations and a large percentage of errors indicate changing algorithms' settings has disrupted the FE model updating process. As per Table 6, the mean MAC and std MAC have been reported as not a number (NaN). This could be due to at least one out-of-range run among the 10 independent runs, which impacted mean values and standard deviations.

According to Table 6, errors on natural frequencies have been extensively extended by minimizing $f_{MAC}(X)$ as the objective function. Therefore, increasing the search agent and maximum iterations could not decrease the discrepancies between the experimental and updated natural frequencies.

The reported results for $f_{NFVAC}(X)$ demonstrate that increasing the search agent and maximum number of iterations have slightly raised the correlation between experimental and updated mode shapes, as shown in Table 6. However, errors on natural frequencies have been expanded and almost doubled compared to the presented results based on the initial algorithms' settings in Table 5.

Comparing Tables 5 and 6 reveals that defining a combined objective function with MAC and NFVAC terms could only reduce discrepancies between experimental and updated natural frequencies. It is important to note that using both algorithms' settings in Tables 5 and 6 has resulted in large standard deviations being reported.

Table 6. Statistical results of FE model updating - IGWO (search agent=10^2 and maximum iteration=10^3)

Mode		1	2	3	4
Experimental f (Hz)		75	204	394	636
$f_{MTMAC}(X)$ $\alpha=1,\beta=1$	mean f (Hz)	75.0002	204.0001	394.0002	635.9997
	std f	4.6807E-04	1.3921E-03	1.2020E-03	5.4034E-03
	error f (%)	2.4385E-04	4.5962E-05	4.8967E-05	4.4825E-05
	mean MAC	0.9996	0.9997	0.9998	0.9999
	std MAC	1.2070E-04	7.9311E-05	7.7271E-05	6.4678E-05
$f_{MTMAC}(X)$ $\alpha=1,\beta=0.5$	mean f (Hz)	75.0000	204.0000	394.0004	635.9990
	std f	6.2225E-04	1.6206E-03	1.2858E-03	4.9290E-03
	error f (%)	1.8190E-05	4.2483E-06	9.6364E-05	1.6088E-04
	mean MAC	0.9997	0.9995	0.9999	0.9999
	std MAC	1.8497E-04	2.0841E-04	3.4103E-05	8.3193E-05
$f_{MTMAC}(X)$ $\alpha=1,\beta=2$	mean f (Hz)	75.0001	204.0004	394.0015	635.9994
	std f	6.3843E-04	1.3020E-03	3.2735E-03	6.6254E-03
	error f (%)	1.7755E-04	1.9738E-04	3.7402E-04	9.6911E-05
	mean MAC	0.9997	0.9997	0.9998	0.9999
	std MAC	7.5283E-05	6.1990E-05	6.2601E-05	5.1168E-05
$f_{MTMAC}(X)$ $\alpha=0.5,\beta=1$	mean f (Hz)	74.9993	204.0001	393.9989	635.9990
	std f	1.5871E-03	1.1847E-03	2.2270E-03	1.4817E-03
	error f (%)	8.8555E-04	4.3998E-05	2.8022E-04	1.5219E-04
	mean MAC	0.9996	0.9996	0.9999	1.0000
	std MAC	1.7648E-04	8.9530E-05	4.4788E-05	1.3229E-05
$f_{MTMAC}(X)$ $\alpha=2,\beta=1$	mean f (Hz)	75.0000	204.0001	394.0031	636.0003
	std f	4.0483E-04	9.0376E-04	7.8134E-03	1.1644E-02
	error f (%)	1.5383E-05	3.7645E-05	7.8092E-04	4.0240E-05
	mean MAC	0.9998	0.9997	0.9997	0.9996
	std MAC	5.1299E-05	8.9985E-05	1.4513E-04	2.9044E-04
$f_{MTMAC}(X)$ $\alpha=5,\beta=1$	mean f (Hz)	74.9999	203.9987	393.9994	634.8819
	std f	1.2821E-04	2.7639E-03	2.5598E-02	**1.5245E+00**
	error f (%)	6.9104E-05	6.4526E-04	1.5048E-04	**1.7580E-01**
	mean MAC	0.9998	0.9997	0.9994	**0.9990**
	std MAC	4.9760E-05	1.0359E-04	2.7398E-04	9.5795E-04
$f_{frequency}(X)$ $\alpha=1,\beta=2$	mean f (Hz)	75.0192	203.9840	393.9928	635.8790
	std f	5.0357E-02	6.4459E-02	1.2240E-01	3.6571E-01
	error f (%)	2.5637E-02	7.8615E-03	1.8233E-03	1.9023E-02
	mean MAC	**0.9371**	**0.9760**	**0.9489**	**0.9952**
	std MAC	1.3138E-01	3.1080E-02	6.3654E-02	4.7472E-03
$f_{frequency}(X)$ $\alpha=2,\beta=2$	mean f (Hz)	1296.2891	1275.5279	1289.3611	1365.5724
	std f	**3.8621E+03**	**3.3885E+03**	**2.8315E+03**	**2.3067E+03**
	error f (%)	**1.6284E+03**	**5.2526E+02**	**2.2725E+02**	**1.1471E+02**
	mean MAC	**NaN**	**NaN**	**NaN**	**NaN**
	std MAC	**NaN**	**NaN**	**NaN**	**NaN**
$f_{MAC}(X)$ $\alpha=1,\beta=2$	mean f (Hz)	47.4772	127.4464	251.0826	389.1929
	std f	**2.4379E+01**	**6.5324E+01**	**1.2969E+02**	**2.0334E+02**
	error f (%)	**3.6697E+01**	**3.7526E+01**	**3.6273E+01**	**3.8806E+01**
	mean MAC	1.0000	1.0000	1.0000	1.0000
	std MAC	9.5927E-06	5.1085E-06	3.0029E-06	4.3548E-06
$f_{NFVAC}(X)$ $\alpha=1,\beta=1$	mean f (Hz)	76.6938	208.6073	402.8981	650.3663
	std f	**1.0757E+01**	**2.9251E+01**	**5.6501E+01**	**9.1206E+01**
	error f (%)	**2.2584E+00**	**2.2585E+00**	**2.2584E+00**	**2.2589E+00**
	mean MAC	**0.9805**	**0.9962**	**0.9897**	**0.9973**
	std MAC	1.8448E-02	2.3080E-03	9.8450E-03	1.7462E-03
$f_{MAC\text{-}NFVAC}(X)$ $\alpha=1,\beta=1$	mean f (Hz)	66.0023	178.0068	349.2904	560.0517
	std f	**4.8665E+00**	**1.2928E+01**	**2.5427E+01**	**4.0993E+01**
	error f (%)	**1.1997E+01**	**1.2742E+01**	**1.1348E+01**	**1.1942E+01**
	mean MAC	0.9999	0.9999	1.0000	1.0000
	std MAC	3.2266E-06	2.1098E-06	1.5568E-06	2.7176E-06

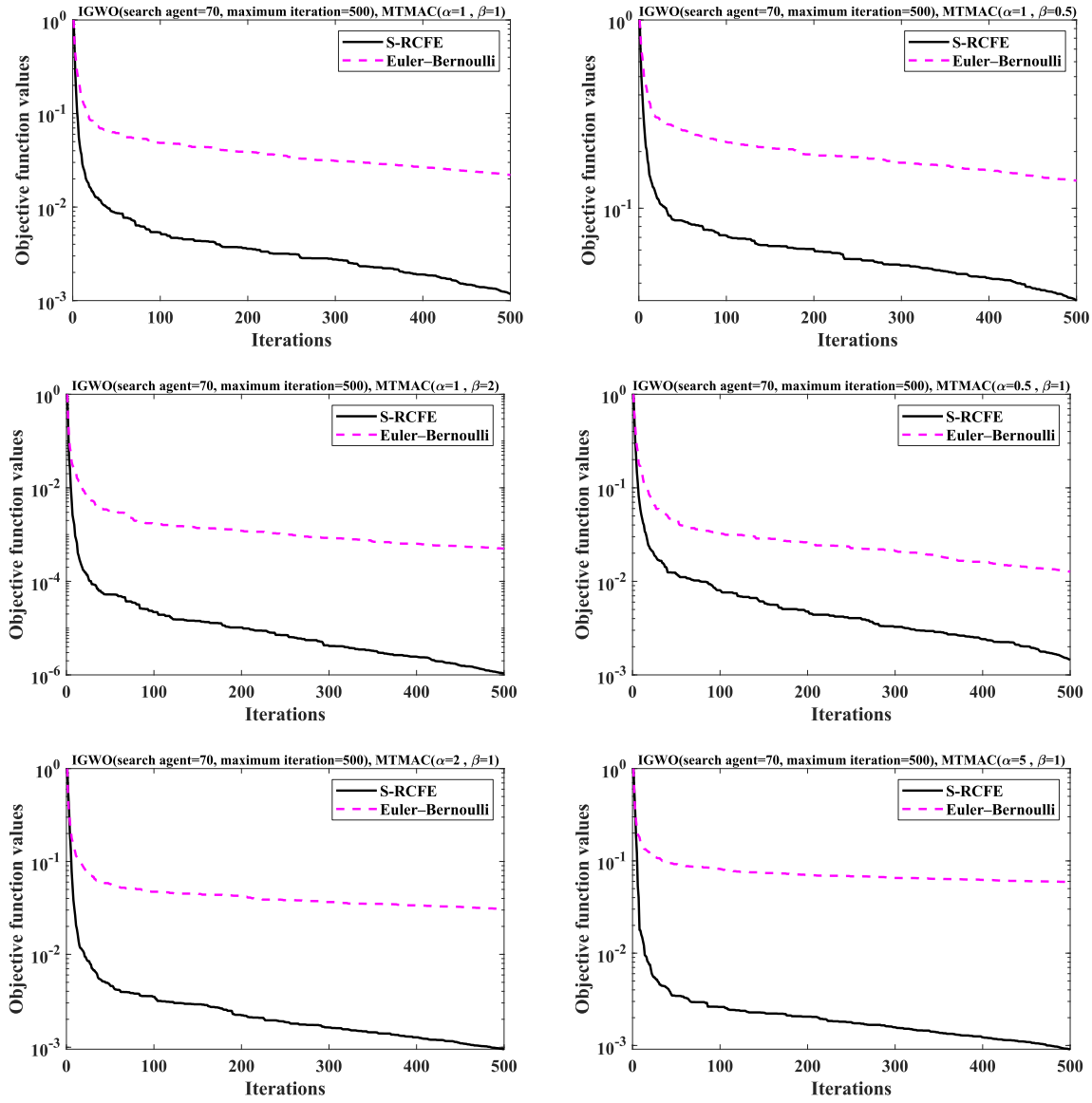

Figure 7. Convergence curves of the IGWO (search agent=70 and maximum iteration=500) for the FE model updating

Figure 7 illustrates the IGWO's convergence curves when using the Euler-Bernoulli beam element and S-RCFE. The mean values of ten independent runs were calculated for each case to provide reliability in comparison. It is clear that the IGWO significantly converges when the FE model is assembled based on S-RCFE. In contrast, the Euler-Bernoulli beam element leads to lower convergence rates. When aiming to minimize an objective function, convergence indicates the objective function's minimization capability and the accuracy of the FE model updating procedure. According to Figure 7, significant differences between the convergence curves of the Euler-Bernoulli beam element and S-RCFE reveal that the S-RCFE with the end fixity factor of each connection as additional design parameters enable us to minimize the objective functions effectively. An assembled FE model based on the Euler-Bernoulli beam element typically considers Young's modulus as design parameters, which might cause lower accuracy in challenging model updating problems.

Tables 7 and 8 have demonstrated that the INFO algorithm could not effectively find optimal solutions for the FE model updating problem regardless of which objective function is employed. It's crucial to understand that the failure of the INFO algorithm does not depend on the value of the search agent and the maximum number of iterations. Additionally, adjusting the coefficients (alpha and beta) could not solve the issue. Based on the statistical analysis accomplished, it is clear that the outcomes of the INFO algorithm have not been acceptable. As per Tables 7 and 8, there are significant differences between the updated and experimental natural frequencies. Besides, the mean MAC and std MAC values are NaN when the objective function is defined as $f_{MTMAC}(X)$, $f_{frequency}(X)$, and $f_{MAC}(X)$. The problem arises due to one or more out-of-range runs among the 10 independent runs. These runs may have significantly impacted the mean values and standard deviations, leading to the current problem.

Tables 7 and 8 show that the INFO algorithm has failed to minimize objective functions based on $f_{NFVAC}(X)$ and $f_{MAC\text{-}NFVAC}(X)$. Adopting an appropriate algorithm for minimizing each objective function is crucial for achieving optimal results, and an inappropriate optimization algorithm may fail to find optimal solutions. One of the possible drawbacks of optimization algorithms is their vulnerability to numerical instability, especially when dealing with large or very small numbers, which can cause the algorithm to fail.

Based on Tables 7 and 8, the INFO algorithm could not provide reliable results by minimizing any of the objective functions, and extremely large standard deviations were obtained in all cases. However, when analyzing statistically, the INFO algorithm may have only one successful solution that smoothed with weaker solutions. Among 10 independent runs, a run with the highest convergence rate is a key indicator for recognizing the best solution. Tables 9 and 10 demonstrate the best results obtained by the INFO algorithm. The results indicate at least one successful solution in updating the FE model using the INFO algorithm and objective functions that rely on MTMAC. The results achieved by the INFO algorithm regarding mode shape correlation and natural frequency agreement are similar to those obtained by the IGWO.

According to Tables 9 and 10, the accuracy of the results is not dependent on objective functions' coefficients. However, adjusting $\alpha = 5$ and $\beta = 1$ has deteriorated the correlation between the updated model and experimental measurements in the fourth mode.

The results presented in Table 9 are quite accurate, indicating that further increasing the search agent to 10^2 and the maximum number of iterations to 10^3, as given in Table 10, would not lead to more accurate results.

Table 7. Statistical results of FE model updating - INFO (search agent=70 and maximum iteration=500)

Mode		1	2	3	4
Experimental f (Hz)		75	204	394	636
$f_{MTMAC}(X)$ $\alpha=1,\beta=1$	mean f (Hz)	1229.7880	1261.5301	1301.3507	1377.0867
	std f	**3.6518E+03**	**3.3442E+03**	**2.8693E+03**	**2.3435E+03**
	error f (%)	**1.5397E+03**	**5.1840E+02**	**2.3029E+02**	**1.1652E+02**
	mean MAC	**NaN**	**NaN**	**NaN**	**NaN**
	std MAC	**NaN**	**NaN**	**NaN**	**NaN**
$f_{MTMAC}(X)$ $\alpha=1,\beta=0.5$	mean f (Hz)	5106.8015	4751.6886	4325.9687	3764.1349
	std f	**6.5003E+03**	**5.8826E+03**	**5.0935E+03**	**4.0523E+03**
	error f (%)	**6.7091E+03**	**2.2293E+03**	**9.9796E+02**	**4.9185E+02**
	mean MAC	**NaN**	**NaN**	**NaN**	**NaN**
	std MAC	**NaN**	**NaN**	**NaN**	**NaN**
$f_{MTMAC}(X)$ $\alpha=1,\beta=2$	mean f (Hz)	6126.7206	5466.8437	4919.8751	4191.1046
	std f	**6.3915E+03**	**5.5625E+03**	**4.7800E+03**	**3.7628E+03**
	error f (%)	**8.0690E+03**	**2.5798E+03**	**1.1487E+03**	**E+025.5898**
	mean MAC	**NaN**	**NaN**	**NaN**	**NaN**
	std MAC	**NaN**	**NaN**	**NaN**	**NaN**
$f_{MTMAC}(X)$ $\alpha=0.5,\beta=1$	mean f (Hz)	6168.4952	5535.7416	4848.3569	4343.8658
	std f	**6.4274E+03**	**5.6275E+03**	**4.7009E+03**	**3.9115E+03**
	error f (%)	**8.1247E+03**	**2.6136E+03**	**1.1305E+03**	**5.8300E+02**
	mean MAC	**NaN**	**NaN**	**NaN**	**NaN**
	std MAC	**NaN**	**NaN**	**NaN**	**NaN**
$f_{MTMAC}(X)$ $\alpha=2,\beta=1$	mean f (Hz)	3740.9623	3499.5424	3265.8769	2945.3140
	std f	**5.9080E+03**	**5.3203E+03**	**4.6267E+03**	**3.7194E+03**
	error f (%)	**4.8879E+03**	**1.6155E+03**	**7.2890E+02**	**3.6310E+02**
	mean MAC	**NaN**	**NaN**	**NaN**	**NaN**
	std MAC	**NaN**	**NaN**	**NaN**	**NaN**
$f_{MTMAC}(X)$ $\alpha=5,\beta=1$	mean f (Hz)	7437.4280	6736.4297	5894.4278	5081.4852
	std f	**6.3619E+03**	**5.6500E+03**	**4.7421E+03**	**3.8394E+03**
	error f (%)	**9.8166E+03**	**3.2022E+03**	**1.3960E+03**	**6.9898E+02**
	mean MAC	**NaN**	**NaN**	**NaN**	**NaN**
	std MAC	**NaN**	**NaN**	**NaN**	**NaN**
$f_{frequency}(X)$ $\alpha=1,\beta=2$	mean f (Hz)	1311.3391	1091.1564	914.4644	1207.0274
	std f	**3.9096E+03**	**2.8054E+03**	**1.6459E+03**	**1.8057E+03**
	error f (%)	**1.6485E+03**	**4.3488E+02**	**1.3210E+02**	**8.9784E+01**
	mean MAC	**NaN**	**NaN**	**NaN**	**NaN**
	std MAC	**NaN**	**NaN**	**NaN**	**NaN**
$f_{frequency}(X)$ $\alpha=2,\beta=2$	mean f (Hz)	1262.2705	1301.2184	1248.7960	1404.0882
	std f	**3.7545E+03**	**3.4697E+03**	**2.7031E+03**	**2.4289E+03**
	error f (%)	**1.5830E+03**	**5.3785E+02**	**2.1695E+02**	**1.2077E+02**
	mean MAC	**NaN**	**NaN**	**NaN**	**NaN**
	std MAC	**NaN**	**NaN**	**NaN**	**NaN**
$f_{MAC}(X)$ $\alpha=1,\beta=2$	mean f (Hz)	2866.2992	2702.9255	2333.8209	2013.5136
	std f	**5.9854E+03**	**5.5449E+03**	**4.6204E+03**	**3.7922E+03**
	error f (%)	**3.7217E+03**	**1.2250E+03**	**4.9234E+02**	**2.1659E+02**
	mean MAC	**NaN**	**NaN**	**NaN**	**NaN**
	std MAC	**NaN**	**NaN**	**NaN**	**NaN**
$f_{NFVAC}(X)$ $\alpha=1,\beta=1$	mean f (Hz)	**Failed**	**Failed**	**Failed**	**Failed**
	std f	**Failed**	**Failed**	**Failed**	**Failed**
	error f (%)	**Failed**	**Failed**	**Failed**	**Failed**
	mean MAC	**Failed**	**Failed**	**Failed**	**Failed**
	std MAC	**Failed**	**Failed**	**Failed**	**Failed**
$f_{MAC\text{-}NFVAC}(X)$ $\alpha=1,\beta=1$	mean f (Hz)	**Failed**	**Failed**	**Failed**	**Failed**
	std f	**Failed**	**Failed**	**Failed**	**Failed**
	error f (%)	**Failed**	**Failed**	**Failed**	**Failed**
	mean MAC	**Failed**	**Failed**	**Failed**	**Failed**
	std MAC	**Failed**	**Failed**	**Failed**	**Failed**

Table 8. Statistical results of FE model updating - INFO (search agent=10^2 and maximum iteration=10^3)

Mode		1	2	3	4
Experimental f (Hz)		75	204	394	636
$f_{MTMAC}(X)$ $\alpha=1,\beta=1$	mean f (Hz)	4858.2876	4459.4887	3986.4284	3594.7637
	std f	**6.1789E+03**	**5.5113E+03**	**4.6475E+03**	**3.8305E+03**
	error f (%)	**6.3777E+03**	**2.0860E+03**	**9.1178E+02**	**4.6521E+02**
	mean MAC	**NaN**	**NaN**	**NaN**	**NaN**
	std MAC	**NaN**	**NaN**	**NaN**	**NaN**
$f_{MTMAC}(X)$ $\alpha=1,\beta=0.5$	mean f (Hz)	4840.8262	4503.5445	4036.1178	3559.2333
	std f	**6.1638E+03**	**5.5687E+03**	**4.7317E+03**	**3.7905E+03**
	error f (%)	**6.3544E+03**	**2.1076E+03**	**9.2440E+02**	**4.5963E+02**
	mean MAC	**NaN**	**NaN**	**NaN**	**NaN**
	std MAC	**NaN**	**NaN**	**NaN**	**NaN**
$f_{MTMAC}(X)$ $\alpha=1,\beta=2$	mean f (Hz)	4855.2513	4586.5111	4031.3948	3607.4482
	std f	**6.2015E+03**	**5.6750E+03**	**4.7058E+03**	**3.8481E+03**
	error f (%)	**6.3737E+03**	**2.1483E+03**	**9.2320E+02**	**4.6721E+02**
	mean MAC	**NaN**	**NaN**	**NaN**	**NaN**
	std MAC	**NaN**	**NaN**	**NaN**	**NaN**
$f_{MTMAC}(X)$ $\alpha=0.5,\beta=1$	mean f (Hz)	7485.8276	6933.2724	6158.6466	5297.7962
	std f	**6.4479E+03**	**5.8471E+03**	**4.9953E+03**	**4.0469E+03**
	error f (%)	**9.8811E+03**	**3.2987E+03**	**1.4631E+03**	**7.3299E+02**
	mean MAC	**NaN**	**NaN**	**NaN**	**NaN**
	std MAC	**NaN**	**NaN**	**NaN**	**NaN**
$f_{MTMAC}(X)$ $\alpha=2,\beta=1$	mean f (Hz)	3691.4617	3410.3106	3124.4446	2860.8126
	std f	**5.8477E+03**	**5.1781E+03**	**4.4078E+03**	**3.5866E+03**
	error f (%)	**4.8219E+03**	**1.5717E+03**	**6.9301E+02**	**3.4981E+02**
	mean MAC	**NaN**	**NaN**	**NaN**	**NaN**
	std MAC	**NaN**	**NaN**	**NaN**	**NaN**
$f_{MTMAC}(X)$ $\alpha=5,\beta=1$	mean f (Hz)	9705.3369	8840.2556	7611.0032	6515.6734
	std f	**5.1108E+03**	**4.5729E+03**	**3.8395E+03**	**3.1220E+03**
	error f (%)	**1.2840E+04**	**4.2335E+03**	**1.8317E+03**	**9.2448E+02**
	mean MAC	**NaN**	**NaN**	**NaN**	**NaN**
	std MAC	**NaN**	**NaN**	**NaN**	**NaN**
$f_{frequency}(X)$ $\alpha=1,\beta=2$	mean f (Hz)	75.0000	204.0000	394.0000	636.0000
	std f	2.1390E-10	8.8324E-11	3.3917E-11	4.1450E-11
	error f (%)	5.0458E-11	1.1954E-11	5.2804E-12	2.4310E-12
	mean MAC	**0.9295**	**0.9729**	**0.9646**	**0.9951**
	std MAC	1.0678E-01	4.8797E-02	5.6533E-02	4.9921E-03
$f_{frequency}(X)$ $\alpha=2,\beta=2$	mean f (Hz)	**2001.2322**	**1837.4670**	**1742.2796**	**1633.3038**
	std f	**4.4091E+03**	**3.8076E+03**	**3.2590E+03**	**2.4878E+03**
	error f (%)	**2.5683E+03**	**8.0072E+02**	**3.4220E+02**	**1.5681E+02**
	mean MAC	**NaN**	**NaN**	**NaN**	**NaN**
	std MAC	**NaN**	**NaN**	**NaN**	**NaN**
$f_{MAC}(X)$ $\alpha=1,\beta=2$	mean f (Hz)	**5180.0121**	**4466.6345**	**4026.2434**	**3364.0542**
	std f	**6.6912E+03**	**5.7334E+03**	**5.1275E+03**	**4.2332E+03**
	error f (%)	**6.8067E+03**	**2.0895E+03**	**9.2189E+02**	**4.2894E+02**
	mean MAC	**NaN**	**NaN**	**NaN**	**NaN**
	std MAC	**NaN**	**NaN**	**NaN**	**NaN**
$f_{NFVAC}(X)$ $\alpha=1,\beta=1$	mean f (Hz)	**Failed**	**Failed**	**Failed**	**Failed**
	std f	**Failed**	**Failed**	**Failed**	**Failed**
	error f (%)	**Failed**	**Failed**	**Failed**	**Failed**
	mean MAC	**Failed**	**Failed**	**Failed**	**Failed**
	std MAC	**Failed**	**Failed**	**Failed**	**Failed**
$f_{MAC\text{-}NFVAC}(X)$ $\alpha=1,\beta=1$	mean f (Hz)	**Failed**	**Failed**	**Failed**	**Failed**
	std f	**Failed**	**Failed**	**Failed**	**Failed**
	error f (%)	**Failed**	**Failed**	**Failed**	**Failed**
	mean MAC	**Failed**	**Failed**	**Failed**	**Failed**
	std MAC	**Failed**	**Failed**	**Failed**	**Failed**

Table 9. Best results of FE model updating among ten runs - INFO (search agent=70 and maximum iteration=500)

Mode		1	2	3	4
Experimental f (Hz)		75	204	394	636
$f_{MTMAC}(X)$ $\alpha=1,\beta=1$	f (Hz)	75.0000	204.0000	394.0000	636.0000
	error f (%)	8.7637E-10	6.5480E-10	8.3967E-12	1.1505E-09
	MAC	0.9996	0.9998	0.9996	0.9993
Best objective function value		1.7121E-03			
$f_{MTMAC}(X)$ $\alpha=1,\beta=0.5$	f (Hz)	75.0000	204.0000	394.0000	636.0000
	error f (%)	2.7241E-10	1.4573E-11	4.6167E-12	3.3069E-12
	MAC	0.9996	0.9996	0.9998	0.9999
Best objective function value		6.2047E-02			
$f_{MTMAC}(X)$ $\alpha=1,\beta=2$	f (Hz)	75.0000	204.0000	394.0000	636.0000
	error f (%)	5.2156E-09	6.4085E-10	9.5207E-08	2.7115E-10
	MAC	0.9996	0.9997	0.9998	0.9995
Best objective function value		4.9064E-07			
$f_{MTMAC}(X)$ $\alpha=0.5,\beta=1$	f (Hz)	75.0000	203.9998	394.0000	636.0000
	error f (%)	1.7347E-06	8.4812E-05	1.8937E-07	7.6496E-08
	MAC	0.9994	0.9994	0.9998	0.9998
Best objective function value		4.8527E-04			
$f_{MTMAC}(X)$ $\alpha=2,\beta=1$	f (Hz)	75.0000	204.0000	394.0000	636.0000
	error f (%)	6.6856E-08	1.6452E-07	6.0668E-08	3.3543E-06
	MAC	0.9996	0.9997	0.9998	0.9995
Best objective function value		5.2434E-03			
$f_{MTMAC}(X)$ $\alpha=5,\beta=1$	f (Hz)	75.0000	204.0000	394.0000	635.9953
	error f (%)	3.5241E-10	5.0309E-11	4.6596E-09	7.3807E-04
	MAC	0.9998	0.9996	0.9997	**0.9958**
Best objective function value		4.1409E-02			

Table 10. Best results of FE model updating among ten runs - INFO (search agent=10^2 and maximum iteration=10^3)

Mode		1	2	3	4
Experimental f (Hz)		75	204	394	636
$f_{MTMAC}(X)$ $\alpha=1,\beta=1$	f (Hz)	75.0000	203.9999	394.0001	636.0000
	error f (%)	1.4093E-05	3.9842E-05	1.5045E-05	7.7018E-06
	MAC	0.9997	0.9997	0.9998	0.9998
Best objective function value		9.5920E-04			
$f_{MTMAC}(X)$ $\alpha=1,\beta=0.5$	f (Hz)	75.0000	204.0000	394.0000	636.0000
	error f (%)	4.9264E-12	1.1006E-12	5.2082E-12	1.1440E-12
	MAC	0.9999	0.9997	0.9998	0.9994
Best objective function value		6.9175E-02			
$f_{MTMAC}(X)$ $\alpha=1,\beta=2$	f (Hz)	75.0000	204.0000	394.0000	636.0000
	error f (%)	1.6729E-10	1.1592E-11	1.0864E-11	5.3090E-12
	MAC	0.9996	0.9997	0.9998	0.9996
Best objective function value		4.3025E-07			
$f_{MTMAC}(X)$ $\alpha=0.5,\beta=1$	f (Hz)	75.0018	204.0000	394.0000	636.0000
	error f (%)	2.3447E-03	6.7652E-06	1.6277E-06	4.4920E-06
	MAC	0.9990	0.9997	0.9999	0.9998
Best objective function value		4.4220E-04			
$f_{MTMAC}(X)$ $\alpha=2,\beta=1$	f (Hz)	75.0000	204.0000	394.0000	636.0000
	error f (%)	4.4281E-10	2.7321E-11	1.8871E-11	4.9693E-12
	MAC	0.9996	0.9999	0.9998	0.9996
Best objective function value		4.6321E-03			
$f_{MTMAC}(X)$ $\alpha=5,\beta=1$	f (Hz)	75.0000	204.0001	393.9581	653.8848
	error f (%)	4.6388E-05	6.1085E-05	1.0642E-02	**2.8121E+00**
	MAC	0.9998	0.9999	0.9999	**0.9981**
Best objective function value		4.4994E-02			

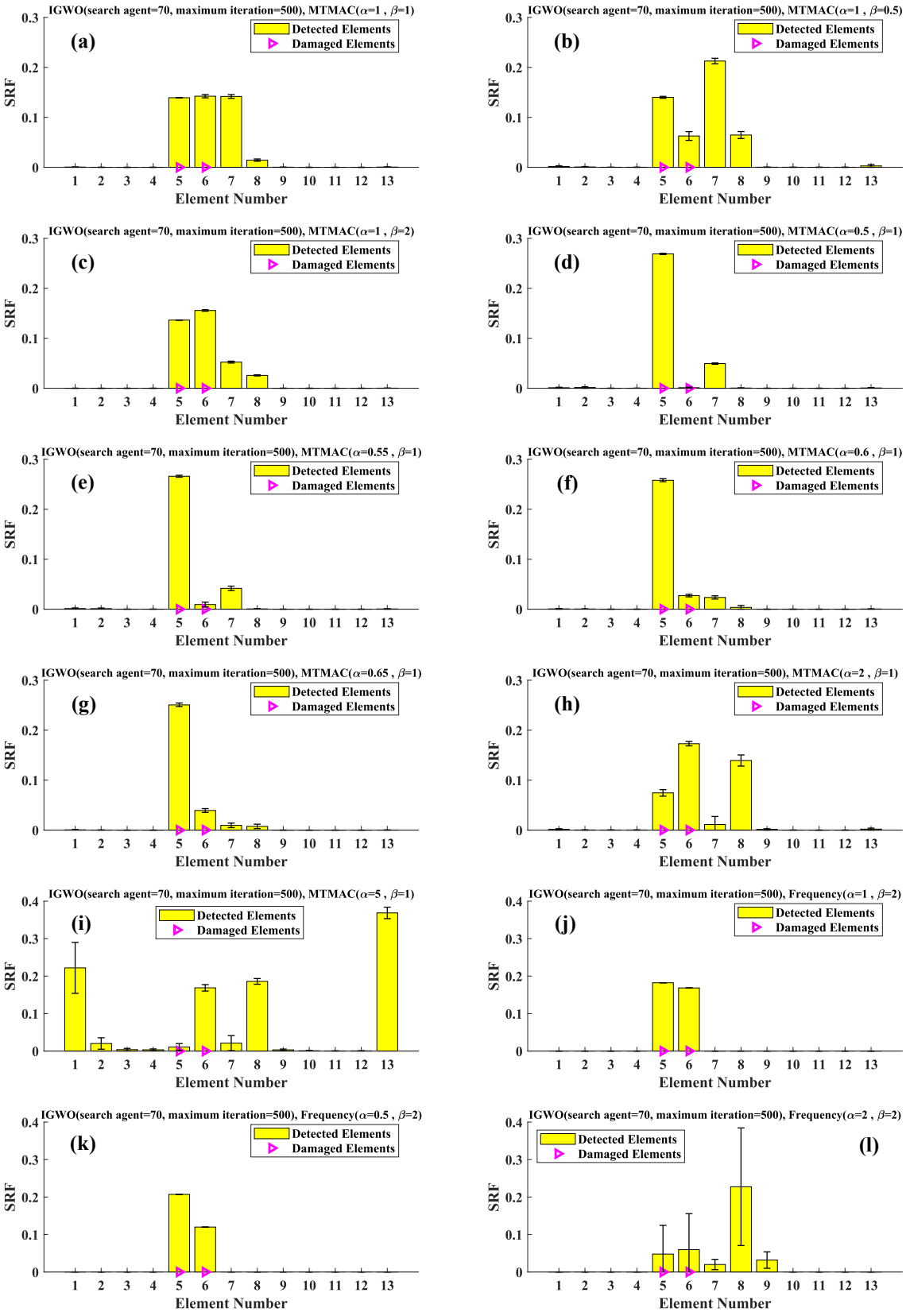

Figure 8. Identified damaged elements and their severities - IGWO (search agent=70 and maximum iteration=500)

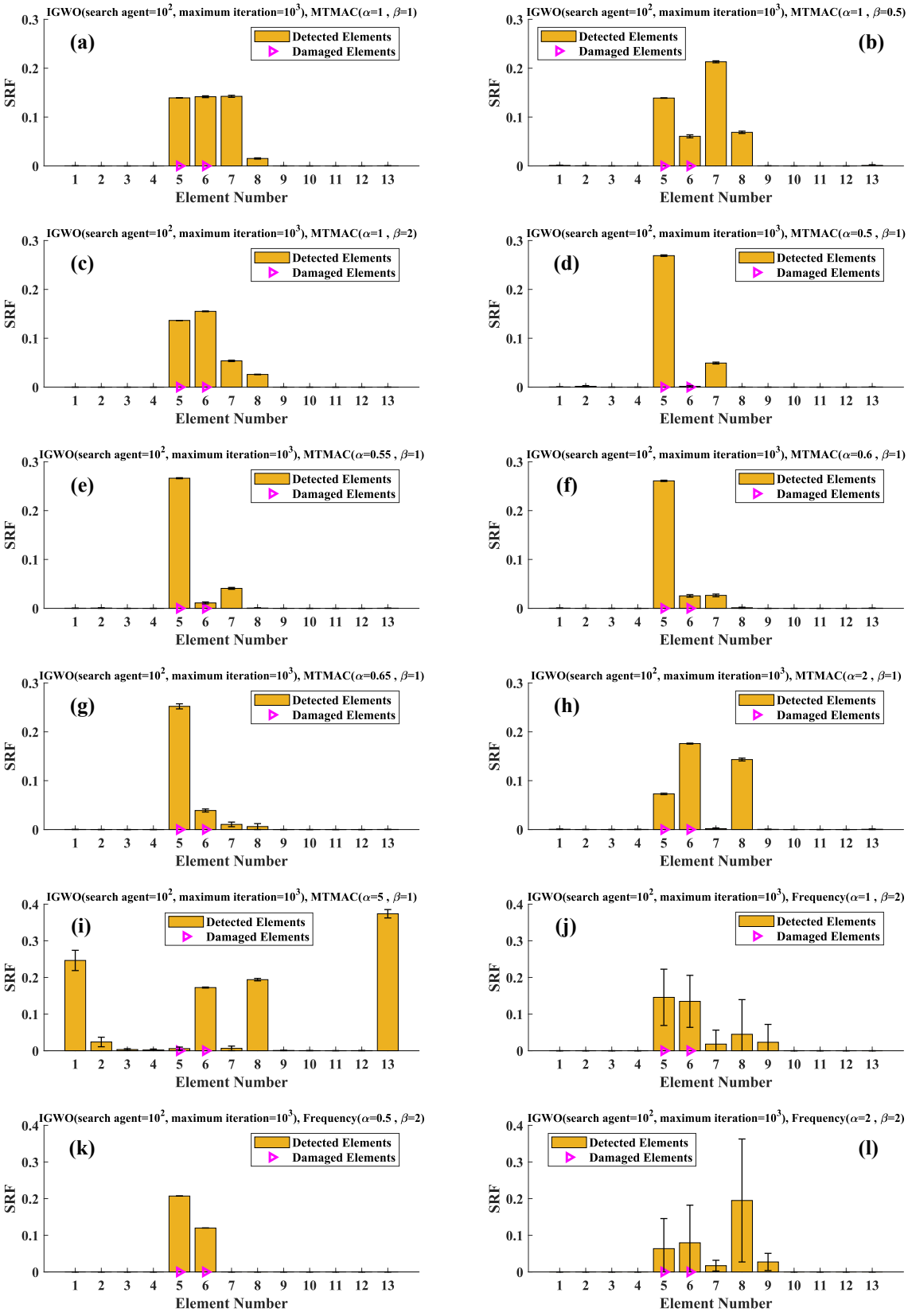

Figure 9. Identified damaged elements and their severities - IGWO (search agent=10^2 and maximum iteration=10^3)

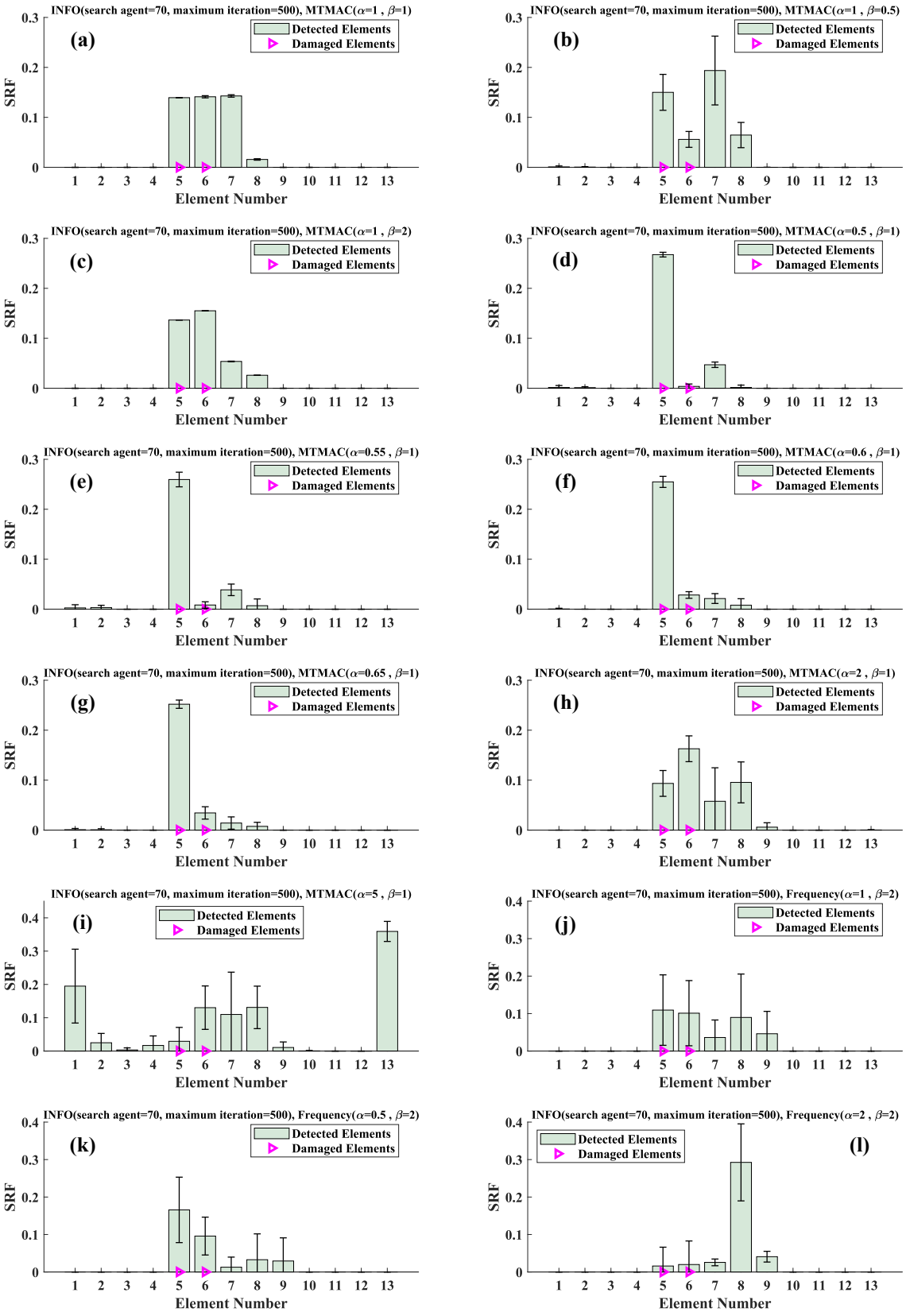

Figure 10. Identified damaged elements and their severities - INFO (search agent=70 and maximum iteration=500)

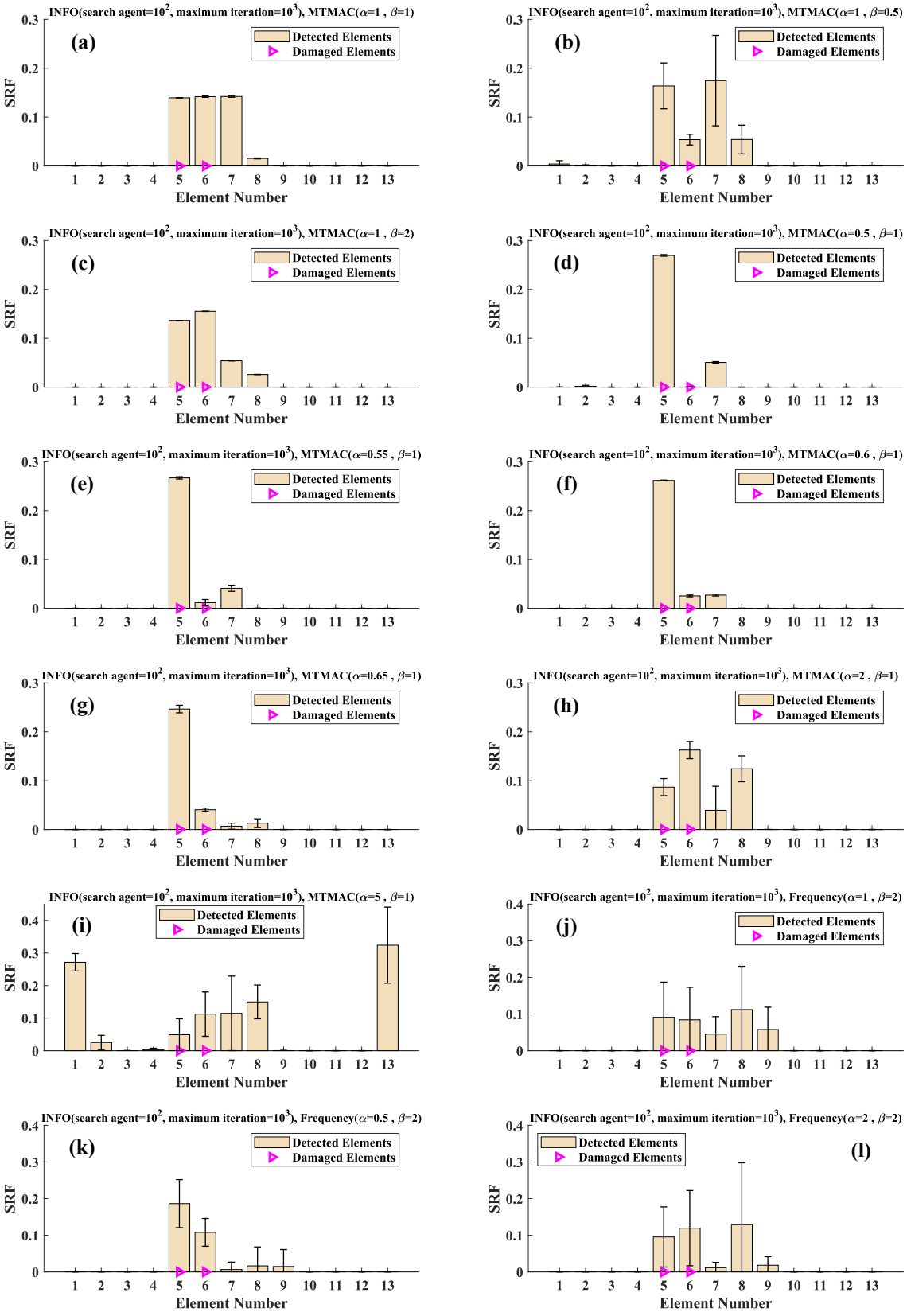

Figure 11. Identified damaged elements and their severities - INFO (search agent=10^2 and maximum iteration=10^3)

Table 11. The performance of objective functions and optimization algorithms for FE model updating and damage detection (✓ Indicates best performances)

Objective functions and coefficients	FE model updating		Damage detection	
	Search agent = 70	Search agent = 10^2	Search agent = 70	Search agent = 10^2
	Maximum iteration = 500	Maximum iteration = 10^3	Maximum iteration = 500	Maximum iteration = 10^3
f_{MTMAC} $\alpha = 1,\ \beta = 1$	IGWO ✓ INFO ●	IGWO ✓ INFO ●	IGWO ● INFO ●	IGWO ● INFO ●
f_{MTMAC} $\alpha = 1,\ \beta = 0.5$	IGWO ✓ INFO ●	IGWO ✓ INFO ●	IGWO ● INFO ●	IGWO ● INFO ●
f_{MTMAC} $\alpha = 1,\ \beta = 2$	IGWO ✓ INFO ●	IGWO ✓ INFO ●	IGWO ● INFO ●	IGWO ● INFO ●
f_{MTMAC} $\alpha = 0.5,\ \beta = 1$	IGWO ✓ INFO ●	IGWO ✓ INFO ●	IGWO ● INFO ●	IGWO ● INFO ●
f_{MTMAC} $\alpha = 0.55,\ \beta = 1$			IGWO ● INFO ●	IGWO ● INFO ●
f_{MTMAC} $\alpha = 0.6,\ \beta = 1$			IGWO ● INFO ●	IGWO ● INFO ●
f_{MTMAC} $\alpha = 0.65,\ \beta = 1$			IGWO ✓ INFO ✓	IGWO ✓ INFO ✓
f_{MTMAC} $\alpha = 2,\ \beta = 1$	IGWO ✓ INFO ●	IGWO ✓ INFO ●	IGWO ● INFO ●	IGWO ● INFO ●
f_{MTMAC} $\alpha = 5,\ \beta = 1$	IGWO ● INFO ●	IGWO ● INFO ●	IGWO ● INFO ●	IGWO ● INFO ●
$f_{frequency}$ $\alpha = 1,\ \beta = 2$	IGWO ● INFO ●	IGWO ● INFO ●	IGWO ● INFO ●	IGWO ● INFO ●
$f_{frequency}$ $\alpha = 0.5,\ \beta = 2$			IGWO ✓ INFO ●	IGWO ✓ INFO ●
$f_{frequency}$ $\alpha = 2,\ \beta = 2$	IGWO ● INFO ●	IGWO ● INFO ●	IGWO ● INFO ●	IGWO ● INFO ●
f_{MAC} $\alpha = 1,\ \beta = 2$	IGWO ● INFO ●	IGWO ● INFO ●		
f_{NFVAC} $\alpha = 1,\ \beta = 1$	IGWO ● INFO ●	IGWO ● INFO ●		
$f_{MAC\text{-}NFVAC}$ $\alpha = 1,\ \beta = 1$	IGWO ● INFO ●	IGWO ● INFO ●		

For statistical visualization of damage detection results, the mean values with plus and minus standard deviations are plotted in Figures 8 to 11. Based on the information provided in Table 3, the damage to the pipe has induced somewhere between 0.8375 m and 1.0375 m from the left end of the pipe. The 2.5-meter length pipe is discretized into 13 elements for FE analysis. The fifth and sixth elements are located within the damaged zone. It's important to mention that the fifth element contains a considerable damage length, and the sixth element includes only a minor damage length. In this paper, the actual severity of damage has not been estimated by theoretical methods. The fracture mechanics approach is typically used to estimate the damage severity, whereas one major drawback of this method is that it relies on relations that are empirically deduced [100]. Therefore, the exact location of the damage is only available to evaluate the performance of the proposed method. However, in the proposed damage detection and severity identification strategy, it is expected that the severity identified for the fifth element will be significantly higher than the stiffness reduction factor identified for the sixth element. Among the presented damage detection results in Figures 8 to 11, Figure 8 (g), Figure 9 (g), Figure 10 (g), and Figure 11 (g) show the most accurate outcomes. These results reveal that minimizing the objective function based on MTMAC and adjusted coefficients alpha = 0.65 and beta=1 through the IGWO and INFO could detect the fifth and sixth elements as damaged. Additionally, the proposed damage detection approach estimates the damage severity as expected for the fifth and sixth elements. At the same time, negligible false alarms have been found for the seventh and eighth elements. Comparing Figures 8 (g) and 9 (g) and Figures 10 (g) and 11 (g) show that increasing the search agent to 10^2 as well as the maximum number of iterations to 10^3 is unnecessary, and both algorithms perform well with initial settings.

Figures 8 (a, b, c, d, e, f, h, and i), Figures 9 (a, b, c, d, e, f, h, and i), Figures 10 (a, b, c, d, e, f, h, and i) and Figures 11 (a, b, c, d, e, f, h, and i) confirm that there are several false identifications when adjusting other coefficients instead of alpha=0.65 and beta=1. Additionally, these figures prove that the IGWO and INFO have the same performance for minimizing objective functions based on MTMAC.

As mentioned in subsection 2.3, natural frequencies are uncomplicated to measure, and this advantage may enable us to develop cost-efficient damage detection tools in real-world applications. Figures 8 (k) and 9 (k) illustrate that employing $f_{frequency}$ (SRF) as an objective function and adjusting alpha = 0.5 and beta =2 could only find the damaged elements without any false identifications. However, the identified stiffness reduction factor for the sixth element should include a minor value because the sixth element contains a negligible cut area. The performance of INFO is relatively lower as compared to IGWO. Figures 10 (k) and 11 (k) show

false identifications for the seventh, eighth, and ninth elements. Besides, identified stiffness reduction factors for the fifth and sixth elements have relatively large standard deviations.

The performance of objective functions and optimization algorithms is summarized in Table 11, considering optimization algorithms' settings for FE model updating and damage detection. A tick mark (✓) indicates the best option or choice among several alternatives.

6. Conclusions

This paper presents an iterative finite element (FE) model updating method to establish a strong correlation between the dynamic characteristics of experimental measurements and those extracted from the FE model in tubular structures. Then, the damage identification step can accurately detect the damaged elements and their severities. The presented iterative FE model updating and damage detection strategies work through minimizing objective functions with adjustable coefficients by newly developed optimization algorithms, including grey wolf optimizer (IGWO) and weIghted meaN oF vectOrs (INFO). The semi-rigidly connected frame element (S-RCFE) was used to assemble the finite element (FE) model of the laboratory scale pipe. The S-RCFE, with further design parameters, facilitates achieving the most tuned FE model and detecting damaged elements with negligible false alarms. The main conclusions of comprehensive statistical analysis for evaluating the efficiency of different objective functions and optimization algorithms can be summarized as follows.

(1) The repeatability of the characteristics extracted from the modal analysis has been examined by analyzing their sensitivity to different hammer impacts. The results show that the standard deviations for at least the first four natural frequencies are exceptionally close to zero, indicating high repeatability.

(2) Incorporating the S-RCFE into the model updating process results in superior convergence rates compared to assembling the FE model using the standard Euler-Bernoulli beam element.

(3) The statistical analysis shows that regardless of the objective functions used, the INFO algorithm is unreliable in updating the FE model. However, it's worth noting that the INFO algorithm yielded at least one successful solution in ten independent runs when MTMAC was defined as the objective function. The IGWO algorithm has provided reliable results with minor standard deviations when defining the MTMAC as the objective function. The results showed that the accuracy of the FE model updating is less dependent on the coefficients of MTMAC, and five out of six objective functions could obtain successful results. The relationship between the updated model and experimental measurements in the fourth mode has been reduced by setting α to 5 and β to 1. The

performance of objective functions based on natural frequency changes, NFVAC, MAC, and MAC-NFVAC, is significantly inadequate.

(4) Both optimization algorithms can entirely minimize the objective function based on MTMAC when adjusting alpha=0.65 and beta=1. Consequently, damaged elements have been identified with much less false alarms. Besides, IGWO could provide promising damage identification results by employing the $f_{frequency}$ *(SRF)* and adjusting alpha=0.5 and beta=2.

(5) A substantial limitation of optimization algorithms that typically leads to inadequate usage of computational resources originates from non-automated parameter tuning and the absence of systematic stopping criteria. A solution to overcome this limitation is using adaptive strategies that dynamically adjust the number of agents or iterations. Therefore, an adaptive version of the grey wolf optimizer is recommended to control the stopping criteria based on the significance of fitness improvement in the optimization process. This version can automatically converge to a sufficiently good optimum in the shortest possible time.

References

1. Esu, O.E., Y. Wang, and M.K. Chryssanthopoulos, *Local vibration mode pairs for damage identification in axisymmetric tubular structures.* Journal of Sound and Vibration, 2021. **494**: p. 115845.
2. Wu, L., J. Mei, and S. Zhao, *Pipeline damage identification based on an optimized back-propagation neural network improved by whale optimization algorithm.* Applied Intelligence, 2022: p. 1-18.
3. Li, D., D. Lu, and J. Hou, *Pipeline damage identification based on additional virtual masses.* Applied Sciences, 2017. **7**(10): p. 1040.
4. Quy, T.B. and J.-M. Kim, *Crack detection and localization in a fluid pipeline based on acoustic emission signals.* Mechanical Systems and Signal Processing, 2021. **150**: p. 107254.
5. Esu, O.E., Y. Wang, and M.K. Chryssanthopoulos, *A baseline-free method for damage identification in pipes from local vibration mode pair frequencies.* Structural health monitoring, 2022. **21**(5): p. 2152-2189.
6. Singh, W.S., S. Thirunavukkarasu, and A. Kumar, *Effect of flaw orientation on magnetic flux leakage and remote field eddy current inspection of small diameter steel tubes.* Nondestructive Testing and Evaluation, 2023. **38**(4): p. 553-571.
7. Peng, X.-L. and H. Hao, *A numerical study of damage detection of underwater pipeline using vibration-based method.* International Journal of Structural Stability and Dynamics, 2012. **12**(03): p. 1250021.
8. Ye, J., et al., *Pipe crack identification based on finite element method of second generation wavelets.* Mechanical Systems and Signal Processing, 2010. **24**(2): p. 379-393.
9. May, Z., M.K. Alam, and N.A. Nayan, *Recent Advances in Nondestructive Method and Assessment of Corrosion Undercoating in Carbon–Steel Pipelines.* Sensors, 2022. **22**(17): p. 6654.
10. Ding, Z., et al., *Vibration-based FRP debonding detection using a Q-learning evolutionary algorithm.* Engineering Structures, 2023. **275**: p. 115254.
11. He, K. and W. Zhu, *Detecting loosening of bolted connections in a pipeline using changes in natural frequencies.* Journal of Vibration and Acoustics, 2014. **136**(3).

12. Naniwadekar, M., S. Naik, and S. Maiti, *On prediction of crack in different orientations in pipe using frequency based approach.* Mechanical systems and signal processing, 2008. **22**(3): p. 693-708.
13. Ghannadi, P. and S.S. Kourehli, *An effective method for damage assessment based on limited measured locations in skeletal structures.* Advances in Structural Engineering, 2021. **24**(1): p. 183-195.
14. Ghannadi, P. and S.S. Kourehli, *Data-driven method of damage detection using sparse sensors installation by SEREPa.* Journal of Civil Structural Health Monitoring, 2019. **9**: p. 459-475.
15. Kourehli, S.S., *Prediction of unmeasured mode shapes and structural damage detection using least squares support vector machine.* Struct. Monit. Maint, 2018. **5**(3): p. 379-390.
16. Rahai, A., F. Bakhtiari-Nejad, and A. Esfandiari, *Damage assessment of structure using incomplete measured mode shapes.* Structural Control and Health Monitoring: The Official Journal of the International Association for Structural Control and Monitoring and of the European Association for the Control of Structures, 2007. **14**(5): p. 808-829.
17. Yan, G., X. Peng, and H. Hao, *Dynamic characteristics of submarine pipelines and experimental validation of a bedding condition assessment approach based on mode-shape curvatures.* Australian Journal of Structural Engineering, 2014. **15**(1): p. 1-13.
18. Altunışık, A.C., et al., *Vibration-based damage detection in beam structures with multiple cracks: modal curvature vs. modal flexibility methods.* Nondestructive Testing and Evaluation, 2019. **34**(1): p. 33-53.
19. Baybordi, S. and A. Esfandiari, *A novel sensitivity-based finite element model updating and damage detection using time domain response.* Journal of Sound and Vibration, 2022. **537**: p. 117187.
20. Baybordi, S. and A. Esfandiari, *Model updating and damage detection of jacket type platform using explicit and exact time domain sensitivity equation.* Ocean Engineering, 2023. **269**: p. 113551.
21. Fathi, A., et al., *Damage detection in an offshore platform using incomplete noisy FRF data by a novel Bayesian model updating method.* Ocean Engineering, 2020. **217**: p. 108023.
22. Esfandiari, A., M.S. Nabiyan, and F.R. Rofooei, *Structural damage detection using principal component analysis of frequency response function data.* Structural Control and Health Monitoring, 2020. **27**(7): p. e2550.
23. Esfandiari, A., et al., *Model updating of a concrete beam with extensive distributed damage using experimental frequency response function.* Journal of Bridge Engineering, 2016. **21**(4): p. 04015081.
24. Standoli, G., et al., *Modal-based FE model updating via genetic algorithms: Exploiting artificial intelligence to build realistic numerical models of historical structures.* Construction and Building Materials, 2021. **303**: p. 124393.
25. Fan, W. and P. Qiao, *Vibration-based damage identification methods: a review and comparative study.* Structural health monitoring, 2011. **10**(1): p. 83-111.
26. Limongelli, M.P., et al., *Vibration response-based damage detection.* Structural Health Monitoring Damage Detection Systems for Aerospace, 2021: p. 133.
27. Avci, O., et al., *A review of vibration-based damage detection in civil structures: From traditional methods to Machine Learning and Deep Learning applications.* Mechanical systems and signal processing, 2021. **147**: p. 107077.
28. Zacharakis, I. and D. Giagopoulos, *Vibration-Based Damage Detection Using Finite Element Modeling and the Metaheuristic Particle Swarm Optimization Algorithm.* Sensors, 2022. **22**(14): p. 5079.
29. Mashayekhi, M. and E. Santini-Bell, *Three-dimensional multiscale finite element models for in-service performance assessment of bridges.* Computer-Aided Civil and Infrastructure Engineering, 2019. **34**(5): p. 385-401.
30. Ereiz, S., I. Duvnjak, and J.F. Jiménez-Alonso. *Review of finite element model updating methods for structural applications*. in *Structures*. 2022. Elsevier.
31. Monchetti, S., et al., *Comparison between Bayesian updating and approximate Bayesian computation for model identification of masonry towers through dynamic data.* Bulletin of Earthquake Engineering, 2024. **22**(7): p. 3491-3509.
32. Sehgal, S. and H. Kumar, *Structural dynamic model updating techniques: A state of the art review.* Archives of Computational Methods in Engineering, 2016. **23**: p. 515-533.

33. Sarmadi, H., A. Karamodin, and A. Entezami, *A new iterative model updating technique based on least squares minimal residual method using measured modal data.* Applied mathematical modelling, 2016. **40**(23-24): p. 10323-10341.
34. Raut, N.P., A. Kolekar, and S. Gombi, *Optimization techniques for damage detection of composite structure: A review.* Materials Today: Proceedings, 2021. **45**: p. 4830-4834.
35. Gomes, G.F., et al., *A review of vibration based inverse methods for damage detection and identification in mechanical structures using optimization algorithms and ANN.* Archives of computational methods in engineering, 2019. **26**: p. 883-897.
36. Bianconi, F., et al., *A genetic algorithm procedure for the automatic updating of fem based on ambient vibration tests.* Sensors, 2020. **20**(11): p. 3315.
37. Salachoris, G.P., et al., *Evolutionary numerical model for cultural heritage structures via genetic algorithms: a case study in central Italy.* Bulletin of Earthquake Engineering, 2024. **22**(7): p. 3591-3625.
38. Ghannadi, P., S.S. Kourehli, and S. Mirjalili, *The application of PSO in structural damage detection: An analysis of the previously released publications (2005–2020).* Frattura ed Integrità Strutturale, 2022. **16**(62): p. 460-489.
39. Ghannadi, P., S. Kourehli, and S. Mirjalili, *A review of the application of the simulated annealing algorithm in structural health monitoring (1995-2021).* Frattura ed Integrità Strutturale, 2023. **64**: p. 51-76.
40. Ghannadi, P., S.S. Kourehli, and A. Nguyen, *The Differential Evolution Algorithm: An Analysis of More than Two Decades of Application in Structural Damage Detection (2001–2022)*, in *Data Driven Methods for Civil Structural Health Monitoring and Resilience*. 2024, CRC Press. p. 14-57.
41. Barontini, A., et al., *An overview on nature-inspired optimization algorithms for Structural Health Monitoring of historical buildings.* Procedia engineering, 2017. **199**: p. 3320-3325.
42. Wang, Z., et al., *A comparative study of common nature-inspired algorithms for continuous function optimization.* Entropy, 2021. **23**(7): p. 874.
43. Nayak, J., et al., *Nature inspired optimization and its application to engineering*. 2021, Springer. p. 1-3.
44. Ghannadi, P. and S.S. Kourehli, *Structural damage detection based on MAC flexibility and frequency using moth-flame algorithm.* Structural Engineering and Mechanics, 2019. **70**(6): p. 649-659.
45. Ghannadi, P. and S.S. Kourehli, *Model updating and damage detection in multi-story shear frames using salp swarm algorithm.* Earthquakes and Structures, 2019. **17**(1): p. 63-73.
46. Ghannadi, P. and S.S. Kourehli, *Multiverse optimizer for structural damage detection: Numerical study and experimental validation.* The Structural Design of Tall and Special Buildings, 2020. **29**(13): p. e1777.
47. Ghannadi, P. and S.S. Kourehli, *Efficiency of the slime mold algorithm for damage detection of large-scale structures.* The Structural Design of Tall and Special Buildings, 2022. **31**(14): p. e1967.
48. Dang, K.D., et al., *A novel model order reduction-based two-stage damage detection paradigm for trusses using time–history acceleration.* Advances in Engineering Software, 2023. **176**: p. 103374.
49. Sang-To, T., et al., *A new movement strategy of grey wolf optimizer for optimization problems and structural damage identification.* Advances in Engineering Software, 2022. **173**: p. 103276.
50. Sang-To, T., et al., *A new metaheuristic algorithm: Shrimp and Goby association search algorithm and its application for damage identification in large-scale and complex structures.* Advances in Engineering Software, 2023. **176**: p. 103363.
51. Minh, H.-L., et al., *Damage identification in high-rise concrete structures using a bio-inspired meta-heuristic optimization algorithm.* Advances in Engineering Software, 2023. **176**: p. 103399.
52. Ding, Z., et al., *A modified Artificial Bee Colony algorithm for structural damage identification under varying temperature based on a novel objective function.* Applied Mathematical Modelling, 2020. **88**: p. 122-141.
53. El-Borgi, S., et al., *Model updating of a scaled piping system and vibration attenuation via locally resonant bandgap formation.* International Journal of Mechanical Sciences, 2021. **194**: p. 106211.

54. Zhu, X., H. Hao, and X. Peng, *Dynamic assessment of underwater pipeline systems using statistical model updating.* International Journal of Structural Stability and Dynamics, 2008. **8**(02): p. 271-297.
55. Wang, Y., et al., *FEM calibrated ARMAX model updating method for time domain damage identification.* Advances in Structural Engineering, 2013. **16**(1): p. 51-60.
56. Rajbamshi, S., Q. Guo, and M. Zhan. *Model updating of fluid-structure interaction effects on piping system*. in *Dynamic Substructures, Volume 4: Proceedings of the 37th IMAC, A Conference and Exposition on Structural Dynamics 2019*. 2020. Springer.
57. Seguini, M., et al. *Experimental and numerical vibration analyses of healthy and cracked pipes*. in *Structural Health Monitoring and Engineering Structures: Select Proceedings of SHM&ES 2020*. 2021. Springer.
58. Seguini, M., et al., *Crack Identification in Pipe Using Improved Artificial Neural Network*, in *Recent Advances in Structural Health Monitoring and Engineering Structures: Select Proceedings of SHM and ES 2022*. 2022, Springer. p. 15-25.
59. Seguini, M., et al., *Crack prediction in pipeline using ANN-PSO based on numerical and experimental modal analysis.* Smart Structures and Systems, 2021. **27**(3): p. 507-523.
60. Xu, Y., et al., *Support condition monitoring of offshore wind turbines using model updating techniques.* Structural health monitoring, 2020. **19**(4): p. 1017-1031.
61. Ren, X., et al., *Support condition monitoring of monopile-supported offshore wind turbines in layered soil based on model updating.* Marine Structures, 2023. **87**: p. 103342.
62. Abdullahi, A. and Y. Wang. *Digital Twin-like Model Updating of a Laboratory Offshore Wind Turbine with Few-Parameters Soil-Structure Interaction Model*. 2021. Proceedings of the 10th International Conference on Structural Health ….
63. Zhang, Z., C. Sun, and V. Jahangiri, *Structural damage identification of offshore wind turbines: A two-step strategy via FE model updating.* Structural Control and Health Monitoring, 2022. **29**(2): p. e2872.
64. Ghannadi, P., et al., *Efficiency of grey wolf optimization algorithm for damage detection of skeletal structures via expanded mode shapes.* Advances in Structural Engineering, 2020. **23**(13): p. 2850-2865.
65. Kahya, V., S. Şimşek, and V. Toğan, *Vibration-based damage detection in anisotropic laminated composite beams by a shear-deformable finite element and harmony search optimization.* Structural and Multidisciplinary Optimization, 2022. **65**(6): p. 181.
66. Ghannadi, P. and S.S. Kourehli, *Investigation of the accuracy of different finite element model reduction techniques.* Structural Monitoring and Maintenance, 2018. **5**(3): p. 417-428.
67. Chen, Y., P. Avitabile, and J. Dodson, *Data consistency assessment function (DCAF).* Mechanical Systems and Signal Processing, 2020. **141**: p. 106688.
68. Nabiyan, M.S., et al., *Mechanics-based model updating for identification and virtual sensing of an offshore wind turbine using sparse measurements.* Structural Control and Health Monitoring, 2021. **28**(2): p. e2647.
69. Cong, S., S.-L.J. Hu, and H.-J. Li, *Using incomplete complex modes for model updating of monopiled offshore wind turbines.* Renewable Energy, 2022. **181**: p. 522-534.
70. Gutiérrez, R., U. Monteiro, and C. Mendonça, *Smoothing and expansion of the experimental mode shapes of an electrical submersible pump.* Ocean Engineering, 2021. **229**: p. 108975.
71. Katkhuda, H.N., H.M. Dwairi, and N. Shatarat, *System identification of steel framed structures with semi-rigid connections.* Structural engineering & mechanics, 2010. **34**(3): p. 351.
72. Nanda, B., D. Maity, and D.K. Maiti, *Modal parameter based inverse approach for structural joint damage assessment using unified particle swarm optimization.* Applied Mathematics and Computation, 2014. **242**: p. 407-422.
73. Hou, R., et al., *Structural damage detection of space frame structures with semi-rigid connections.* Engineering Structures, 2021. **235**: p. 112029.
74. Pahnabi, N. and S.M. Seyedpoor, *Damage identification in connections of moment frames using time domain responses and an optimization method.* Frontiers of Structural and Civil Engineering, 2021. **15**(4): p. 851-866.
75. Aval, S.B.B. and P. Mohebian, *Joint damage identification in frame structures by integrating a new damage index with equilibrium optimizer algorithm.* International Journal of Structural Stability and Dynamics, 2022. **22**(05): p. 2250056.

76. Ghannadi, P., et al. *Finite element model updating and damage identification using semi-rigidly connected frame element and optimization procedure: An experimental validation*. in *Structures*. 2023. Elsevier.
77. Entezami, A., H. Shariatmadar, and S. Mariani, *Early damage assessment in large-scale structures by innovative statistical pattern recognition methods based on time series modeling and novelty detection.* Advances in Engineering Software, 2020. **150**: p. 102923.
78. Wang, X., et al., *Structural damage detection based on cross-correlation function with data fusion of various dynamic measurements.* Journal of Sound and Vibration, 2022. **541**: p. 117373.
79. Wang, S., *Model updating and parameters estimation incorporating flexible joints and boundary conditions.* Inverse Problems in Science and Engineering, 2014. **22**(5): p. 727-745.
80. Xue-Lin, P., *Condition Monitoring of Offshore Pipelines Using Vibration Based Methods*. 2012.
81. Hernández González, I., *Damage identification of large-scale structures using surrogate kriging models and particle swarm algorithms*. 2022.
82. Qin, S., et al., *Improved Metaheuristic Algorithm Based Finite Element Model Updating of a Hybrid Girder Cable-Stayed Railway Bridge.* Buildings, 2022. **12**(7): p. 958.
83. Shabbir, F., et al., *Structural damage detection with different objective functions in noisy conditions using an evolutionary algorithm.* Applied Sciences, 2017. **7**(12): p. 1245.
84. Du, D.-C., et al., *Efficiency of Jaya algorithm for solving the optimization-based structural damage identification problem based on a hybrid objective function.* Engineering Optimization, 2018. **50**(8): p. 1233-1251.
85. Georgioudakis, M. and V. Plevris, *A combined modal correlation criterion for structural damage identification with noisy modal data.* Advances in Civil Engineering, 2018. **2018**.
86. Perera, R., A. Ruiz, and C. Manzano, *Performance assessment of multicriteria damage identification genetic algorithms.* Computers & Structures, 2009. **87**(1-2): p. 120-127.
87. Pastor, M., M. Binda, and T. Harčarik, *Modal assurance criterion.* Procedia Engineering, 2012. **48**: p. 543-548.
88. Chopra, A.K., *Dynamics of structures*. 2007: Pearson Education India.
89. Yang, Z. and L. Wang, *Structural damage detection by changes in natural frequencies.* Journal of intelligent material systems and structures, 2010. **21**(3): p. 309-319.
90. Hofmeister, B., *Vibration-based damage localisation: Impulse response identification and model updating methods.* Mitteilungen des Instituts für Statik und Dynamik der Leibniz Universität Hannover; 51, 2023.
91. Yang, X.-S., *Chapter 14 - Multi-Objective Optimization*, in *Nature-Inspired Optimization Algorithms*, X.-S. Yang, Editor. 2014, Elsevier: Oxford. p. 197-211.
92. Park, H.S., J. Kim, and B.K. Oh, *Model updating method for damage detection of building structures under ambient excitation using modal participation ratio.* Measurement, 2019. **133**: p. 251-261.
93. Caicedo, D., L.A. Lara-Valencia, and J. Brito, *Frequency-based methods for the detection of damage in structures: A chronological review.* Dyna, 2021. **88**(218): p. 203-211.
94. Kim, J.-T., et al., *Damage identification in beam-type structures: frequency-based method vs mode-shape-based method.* Engineering structures, 2003. **25**(1): p. 57-67.
95. Ahmadianfar, I., et al., *INFO: An efficient optimization algorithm based on weighted mean of vectors.* Expert Systems with Applications, 2022. **195**: p. 116516.
96. Singla, M.K., et al., *An enhanced efficient optimization algorithm (EINFO) for accurate extraction of proton exchange membrane fuel cell parameters.* Soft Computing, 2023. **27**(14): p. 9619-9638.
97. Mirjalili, S., S.M. Mirjalili, and A. Lewis, *Grey wolf optimizer.* Advances in engineering software, 2014. **69**: p. 46-61.
98. Nadimi-Shahraki, M.H., S. Taghian, and S. Mirjalili, *An improved grey wolf optimizer for solving engineering problems.* Expert Systems with Applications, 2021. **166**: p. 113917.
99. Esu, O.E., *Vibration-based indicators for damage identification in axisymmetric structures*. 2022, University of Surrey.
100. Nitescu, C., et al. *Damage severity estimation from the global stiffness decrease*. in *Journal of Physics: Conference Series*. 2017. IOP Publishing.